NASA Contractor Report 187630

ICASE INTERIM REPORT 19

PROCEEDINGS FOR THE ICASE WORKSHOP ON HETEROGENEOUS BOUNDARY CONDITIONS

A. Louise Perkins
Jeffrey S. Scroggs

NASA Contract No. NAS1-18605
August 1991

INSTITUTE FOR COMPUTER APPLICATIONS IN SCIENCE AND ENGINEERING
NASA Langley Research Center, Hampton, Virginia 23665

Operated by the Universities Space Research Association

National Aeronautics and
Space Administration

Langley Research Center
Hampton, Virginia 23665-5225

ICASE INTERIM REPORTS

ICASE has introduced a new report series to be called ICASE Interim Reports. The series will complement the more familiar blue ICASE reports that have been distributed for many years. The blue reports are intended as preprints of research that has been submitted for publication in either refereed journals or conference proceedings. In general, the green Interim Report will not be submitted for publication, at least not in its printed form. It will be used for research that has reached a certain level of maturity but needs additional refinement, for technical reviews or position statements, for bibliographies, and for computer software. The Interim Reports will receive the same distribution as the ICASE Reports. They will be available upon request in the future, and they may be referenced in other publications.

Robert G. Voigt
Director

OMIT

PROCEEDINGS FOR THE ICASE WORKSHOP ON HETEROGENEOUS BOUNDARY CONDITIONS*

A. Louise Perkins
Massachusetts Institute of Technology
and
Jeffrey S. Scroggs
North Carolina State University

ABSTRACT

Domain Decomposition is a complex problem with many interesting aspects. The choice of decomposition can be made based on many different criteria, and the choice of interface of internal boundary conditions are numerous. Even more interesting from a modeling perspective is that the various regions under study may have different dynamical balances, indicating that different physical processes are dominating the flow in those regions. It may be desirable to use different numerical approximations in the regions where the physical processes are dominated by different balances.

The Institute for Computer Applications in Science and Engineering (ICASE), recognizing the need to more clearly define the nature of these complex problems, sponsored this workshop on Heterogeneous Boundary Conditions at the NASA Langley Research Center in Hampton, Virginia. This proceedings is an informal collection of the presentations and discussion groups. It also includes a bibliography that contains many of the references that discuss related topics.

The proceedings begins with summaries of the discussion groups. Then papers describing the talks are presented. Lastly, the bibliography is included, and an index by subject is provided.

*This workshop was sponsored by the Institute for Computer Applications in Science and Engineering (ICASE) at the National Aeronautics and Space Administration (NASA) at the Langley Research Center, Hampton, VA 23665.

Contents

Visual Artifacts

Discussion Leader: Bill Gropp
Argonne National Laboratory
Report by: A. Louise Perkins
Massachusetts Institute of Technology

The discussion began with Dr. Bill Gropp introducing the concept of visual artifacts in numerical solutions. He presented examples of errors that appeared to be significant to the human eye, but that were well below the error criteria for the problem, and did not impact the quality of the numerical solution.

The discussion then focused on defining a model problem where visual artifacts could be examined explicitly.

Model Problem

A. Louise Perkins
Massachusetts Institute of Technology

1 Introduction

At the ICASE Workshop on Heterogeneous Boundary Conditions a general optics problem that allows interference was suggested for study. The large-scale interference pattern that develops is quite sensitive to small perturbations in the boundary conditions. Hence it seemed ideal for testing and observing errors due to grid interface effects introduced by domain decomposition methods. Although the problem specification is somewhat arbitrary, it is necessary to be specific in order to compare results because it is expected that several researchers will explore this problem.

2 Error Measurements

The interference that we wish to test lends itself to error analysis using both a visual as well as more standard numerical acceptance criteria. The more standard numerical criteria are

- propagation error
- L_1 error
- L_2 error
- L_∞ error

By propagation error we mean the phase difference between the computed location of the wave front and the exact location of the same wave front.

Visually this problem gives rise to an interference pattern that can be compared for sharpness as well as location. We are interested in seeing these differences across the artificial interfaces introduced by the decomposition.

3 Motivation

Dr. Bill Gropp suggested we examine a problem that had visual meaning in its errors, to allow studying the types of errors introduced between refined and coarse meshes at a more intuitive level. He suggested an optics interference problem.

4 Optical Interference

Fermats' principle of least time is recast in Feynman et. al. [1] briefly from a quantum-dynamical perspective. By considering "rays of light" as photons, the ray path can be considered a sum of the individual paths of the photons. The ray path is then defined by the probability of each photon taking different paths.

Upon encountering a barrier that contains a wide slit, a wave will continue through the slit almost undisturbed and geometric optics is a good model for ray behavior. But when the slit is sufficiently reduced in size, the choices for photon paths are truncated, and the probability distribution is altered, affecting the geometry of the wave front as it passes through the slit.

This behavior is more easily understood by considering the simpler, less accurate, but more intuitive, Huygens principle which states that "all points on a wavefront can be considered as point sources for the production of spherical secondary wavelets. After a time the new position of the wavefront will be the surface of tangency to these secondary wavelets", as described in Halliday and Resnick [2]. Considering this simplified wave theory of light, a barrier in a wave path with a slit on the order of the wave length will cause diffraction. That is, the end points allowed to pass through the slit will no longer have symmetrical wavelets on either side, and they will bend at the ends.

Placing two slits aside each other will replicate the limiting behavior twice, and the resulting wave patterns will interact, causing interference. The interference pattern will be visible, and dependent upon the original wave frequency. This interference pattern is quite sensitive to phase errors, so that the choice of grid sizes influences the solution behavior. This is the interesting aspect of this problem.

5 The Interference Pattern

Consider the wave equation

$$\frac{\partial^2 u}{\partial t^2} = \Delta u.$$

Here Δ is the Laplacian. In the positive quadrant place two slits along the x-axis at locations x_1 and x_2, with

$$d = x_2 - x_1.$$

Here x_1 and x_2 are the mid-points of the two slits. Then for any point in the quadrant, $P = (x_p, y_p)$, let d_1 be the distance from x_1 to P, and d_2 be the distance from x_2 to P.

Waves will arrive at P out of phase due to the difference in the path lengths d_1 and d_2. The maximum interference will occur when

$$|d_2 - d_1| = m\lambda$$

where λ is the original incident plane wavelength and m is a nonnegative integer. The minimum, of course, occurs at the half distances $(m + \frac{1}{2})$.

The size of our slits can now be specified. They should be at most of width λ. A slit width less than or equal to the incident wavelength is sufficiently small to diffract the wave on a visible scale. This problem is interesting because generation of the large scale pattern depends on how accurately the small scale dynamics has been captured about the slits.

6 Geometry

Here we assume that the problem has been normalized so that

$$x_l = 0,$$

$$x_r = 1,$$

$$y_b = 0,$$

$$y_t = 1,$$

We arbitrarily choose $x_1 = \frac{1}{2} - 5\lambda$, $x_2 = \frac{1}{2} + 5\lambda$. This geometry is illustrated on the following page in Fig. 1.

7 Initial Conditions

The initial region, including all boundaries except the slits, should be quiescent ($u = 0$).

Prescribe a plane wave described by the following function:

$$sin\frac{2\pi}{\lambda}(y - vt) \tag{7.1}$$

where λ is the wavelength and v is the phase velocity. This impacts our domain along the slits $[\frac{1}{2} - 5.5\lambda, \frac{1}{2} - 4.5\lambda]$ and $[\frac{1}{2} + 4.5\lambda, \frac{1}{2} + 5.5\lambda]$ of the x-axis for all time $t > 0$. Here, the equation reduces to

$$sin\frac{2\pi}{\lambda}(-vt). \tag{7.2}$$

The phase velocity is known, allowing radiative boundary conditions to be defined. This is done in the section 9.

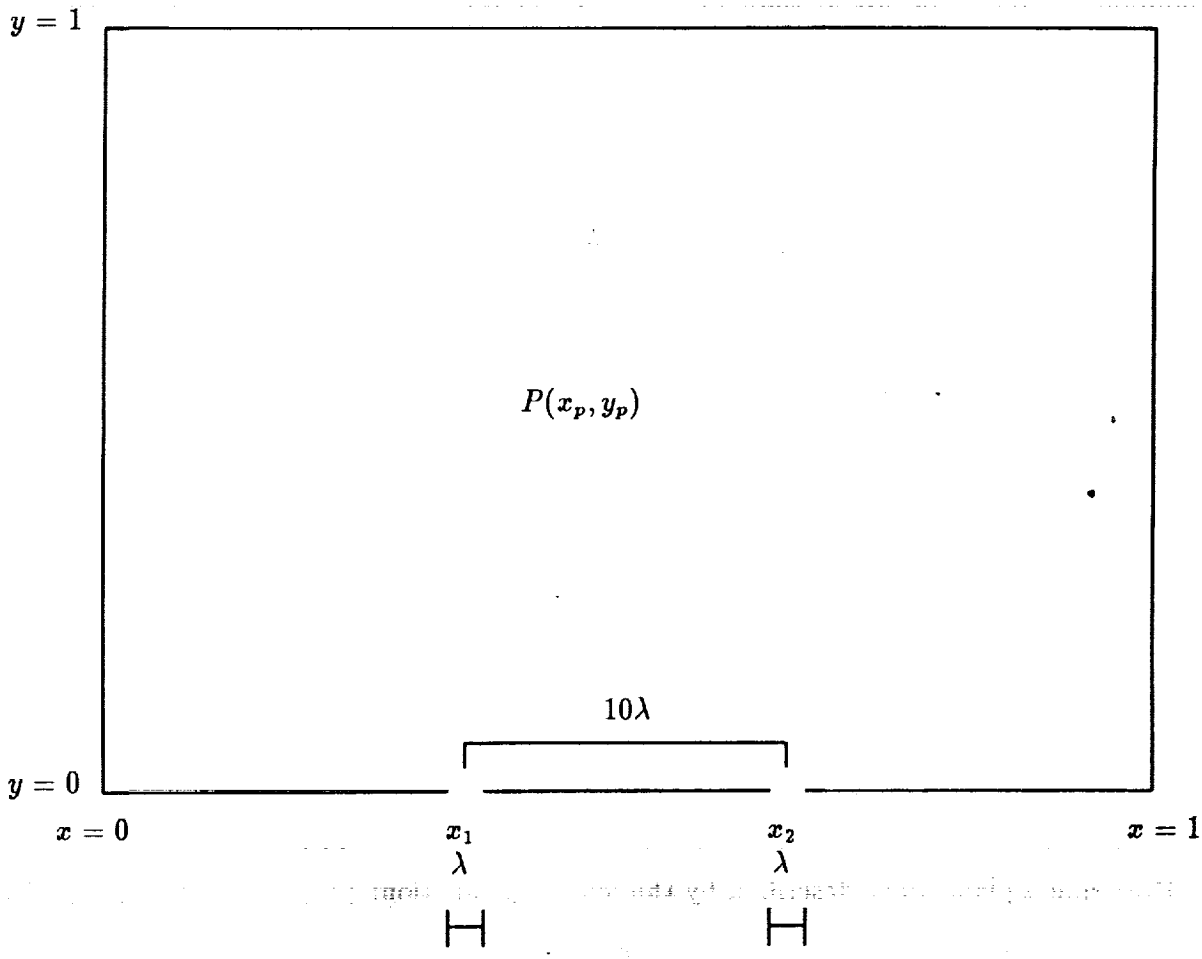

Figure 6.1: Problem Domain

8 Exact Solution

The exact interference pattern is the superposition of the two waves. For any point $P(x,y)$ in the domain, the travel time to P will be different from the two slits. Let the time from slit x_i be t_i. Then the value at P will be the sum of the P_i where

$$P_i(x,y) = sin\frac{2\pi}{\lambda}(-v(t-t_i))$$

for $(t-t_i) \geq 0$ and zero otherwise. We note that the distance from slit x_i to the point $P(x,y)$ is

$$d_i = ((x-x_i)^2 + y^2)^{\frac{1}{2}}.$$

9 Boundary Conditions

All boundaries, except the slits which are prescribed with the incoming plane wave, evolve with the solution. Any workable boundary conditions can be applied on these boundaries, with the goal that these boundary conditions should influence the interference pattern as little as possible.

For our prescribed incident plane wave we have the exact solution. However, prescription of these exact boundary values on our numerical approximation of the solution could cause the numerical approximation to degrade. Hence we recommend radiative boundary conditions because we know the phase velocity exactly and hope that the numerical phase velocity is quite close to the correct one. Then an open boundary condition can be used that advects the interference pattern out of the domain by advancing the wave equation,

$$\frac{\partial u}{\partial t} + v\frac{\partial u}{\partial n} = 0$$

where n is the direction normal to the boundary.

10 Domain Decomposition Method

Our purpose in examining this test problem is to measure directly the effect of mesh refinement and the resulting mesh interfaces on a known wave that is sensitive to phase errors, while concurrently being able to visually display a meaningful picture of the effects of the refinement-induced error on the solution.

The Coarse mesh must be able to adequately represent the interference pattern for the visual comparisons. It should be no larger than $\Delta x = \Delta y = \frac{\lambda}{4}$, and may need to be smaller. The workshop suggested $\frac{\lambda}{10}$. We suggest that $\frac{\lambda}{4}$, $\frac{\lambda}{10}$ and $\frac{\lambda}{20}$ all be tested. However, these values are only *apriori* suggestions as we have not yet worked this problem.

The refined mesh must be able to adequately capture the diffraction behavior, so that the plane wave front "bends" as it passes through the slit. Given that the coarse and refined

meshes are sufficiently accurate, the phase errors introduced during the problem solution will be a function of the sound speed on the two grids plus the coarse/refined grid interaction errors.

Due to the geometry of the problem, non-adaptive local uniform mesh refinement is adequate for the domain decomposition.

11 Discretization

We suggest a second order in space and time Leap Frog/Hopscotch discretization method should be used. We anticipate beginning with $\lambda = 0.1$, and $\lambda = 0.05$.

12 Analysis

We expect that calculations for boundary errors and the ratio of mesh refinements will be analyzed. These can be done both analytically and by comparison to an everywhere fine mesh.

References

[1] R.P. Feynman, R.B. Leighton, and M. Sands, *The Feynman Lectures On Physics Mainly Mechanics, Radiation, and Heat*, Addison-Wesley, (26-8), 1963.

[2] D. Halliday, and R. Resnick, *Fundamentals of Physics*, John Wiley and Sons, 1970.

Discussion Summary: Fictitious Domain Methods

Discussion Leader: Rowland Glowinski
University of Texas at Houston
Report by: Garry Rodrigue
University of California at Davis

Fictitious Domain methods are constructed in the following manner: Suppose a partial differential equation is to be solved on an open bounded set Ω in two or three dimensions. Let R be a rectangular domain containing the closure of Ω. The partial differential equation is first solved on R. Using the solution on R, the solution of the equation on Ω is then recovered by some procedure.

The advantage of the fictitious domain method is that in many cases the solution of a partial differential equation on a rectangular region is easier to compute than on a non-rectangular region. Not only do more accurate algorithms exist for rectangular regions but they are also more computationally efficient. The difficulty in the method, of course, is the procedure that is used to tie the "global" solution on R to the "local" solution on Ω. This is generally where the inefficiencies of the method creep in and where most of the current research on the method is being done. A classic application of a fictitious domain method is the computation of the solution of an elliptic partial differential equation on a general region. Here, the global solution on a rectangular region can be computed by a fast Poisson solver. These solvers are quite effecient for rectangular regions but not for other geometries. The global solution is tied to the local solution on the general region via ideas in capcitance matrix techniques. A discusion of this approach is given in [1]. Other uses of fictitious domain methods are given in the remaining references.

Fictitious domain methods for solving elliptic PDEs on general regions are also very efficient when used on a parallel computer. The reason for this is that one can use the many domain decomposition methods that are available for solving the PDE on the fictitious rectangular region. In domain decomposition methods, the global rectangle is decomposed into sub-rectangles of equal size and elliptic PDEs are solved on each sub-rectangle to provide approximations to the elliptic PDE on the global rectangle This process is iterated upon several times to get successively better approximations, see references in [4]. This is significant in that the approximations on the sub-rectangles can often be computed simultaneously and, thus, can be carried out in parallel on the individual processors of a multiprocessor. Moreover, because the approximations to the global equation are furnished by the solutions of PDEs on sub-rectangles of equal size, they can be calculated in the same amount of time. This is advantageous because the load balancing and synchronization overhead incurred from managing the tasks of computing the approximations on the processors becomes almost non-existent.

The discussion on fictitious domain methods began with a short talk by Roland Glowinski where he gave some examples of a variational approach to fictitious domain methods for solving the Helmholtz and Navier-Stokes equations. After Glowinski's introduction to the subject, the question of the usefulness of the method was tossed out to the audience. A

comment was made that the fictious domain method seems to be the only reasonable way of solving three-dimensional partial differential equations on general domains. This statement was justified by the admission by several people that the implementations of standard finite element or finite difference techniques to 3-D problems is a horrendous task. There was a considerable amount of discussion on this point but, in the end, the audience agreed that the fictitious domain method is a viable approach to three-dimensional problems and more research is needed in this area.

References

[1] Borgers, C.: Domain imbedding methods for the Stokes equations. Numerische Mathematik 57, 435-451 (1990)

[2] Buzbee, B.L., Dorr, F.W., George, J.A., Golub, G.H.: The direct solution of the discrete Poisson equation on irregular regions. SIAM J. Numeri. Anal. 8, 772-736 (1971)

[3] Dryja, M.: A finite element capacitance matrix method for the elliptic problem. SIAM J. Numer. Anal. 20,671-680 (1983)

[4] Glowinski, R.: Fictitious domain/Lagrange multiplier methods for the solution of partial differential equations. Proceedings of Fifth Conference on Domain Decomposition Methods for Partial Differential Equations, Norfolk Va., SIAM Pub., 1990

[5] Marchuk, G. I., Kuznetsov, Y. A., Matsokin, A.M.: Fictitious domain and domain decomposition methods. Sov. J. Numer. Anal. Math. Modelling 1, 3 - 61 (1986)

[6] Proskurowski, W.: Numerical solution of Helmholtz's equation by implicit capaciatance matrix methods. ACM Trans. Math. Software 5, 36-49 (1979)

Domain-Decomposed Preconditionings for Transport Operators†

Tony F. Chan* — CD1U6017
William D. Gropp** - AX337235
and
David E. Keyes*** - YE661058

Abstract

We test the performance of five different interface preconditionings for domain-decomposed convection-diffusion problems, including a novel one known as the spectral probe, while varying mesh parameter, Reynolds number, ratio of subdomain diffusion coefficients, and domain aspect ratio. The preconditioners are representative of the range of practically computable possibilities that have appeared in the domain decomposition literature for the treatment of nonoverlapping subdomains. We demonstrate through a large number of numerical examples that no single preconditioner can be considered uniformly superior or uniformly inferior to the rest, but that knowledge of particulars, including the shape and strength of the convection, is important in selecting among them in a given problem.

1. Introduction

The solution of linearized convection-diffusion equations of the form

$$\vec{c} \cdot \nabla \phi - \nabla \cdot \epsilon \nabla \phi = f, \tag{1.1}$$

where ϕ is a conserved quantity (energy, mass fraction, momentum component, etc.) transported under the influence of velocity field $\vec{c}$ and diffusivity ϵ is required throughout computational physics. Discretization by finite differences or finite elements results in a large sparse system of algebraic equations whose solution can be demanding in computational resources and is one of the many driving forces for parallel computation. Because the strength of coupling between a pair of discrete unknowns governed by an equation like (1.1) decays with physical separation (more or less isotropically depending upon $\vec{c}$), it is natural to partition the problem spatially when looking for concurrency in the solution algorithm. Parallelism is, in fact, only one of several compelling reasons for the recent surge of research on domain decomposition algorithms exemplified by the volumes [9, 10, 17]. Others include a powerful theory describing optimal or near-optimal algebraic convergence rates for hierarchical preconditioners of domain-decomposed type, the convenience of composite array data structures for describing complex shapes, a desire to employ solution techniques and quality

†This report is an augmentation of a report entitled *Interface Preconditioning for Domain-Decomposed Convection-Diffusion Operators* by the first and third authors that appeared in "Proceedings of the Third International Symposium on Domain Decomposition Methods," T. F. Chan, R. Glowinski, J. Periaux, and O. B.Widlund, eds., pp. 245-262, SIAM, 1990.

*Department of Mathematics, UCLA, Los Angeles, CA 90024. The work of this author was supported in part by NSF ASC 9003002, DOE DE-FG03-87ER25037, and ARO DAAL03-88-K-0085.

**Mathematics and Computer Science Division, Argonne National Laboratory, Argonne, IL 60439. The work of this author was supported in part by the Applied Mathematical Sciences subprogram of the Office of Energy Research, U.S. Department of Energy, under Contract W-31-109-ENG-38.

***Department of Mechanical Engineering, Yale University, New Haven, CT 06520. The work of this author was supported in part by NSF ECS-8957475 and by the National Aeronautics and Space Administration under NASA Contract NAS1-18605, while the author was in residence at the Institute for Computer Applications in Science and Engineering, NASA-Langley Research Center, Hampton, VA 23665.

software restricted to problems with various local uniformity requirements (which are subproblems with regard to (1.1)), and sheer problem size, which can ultimately push numerical ill-conditioning and serial memory traffic beyond acceptable limits.

Preconditionings for interfacial degrees of freedom have been the focus of much attention during the development of domain decomposition methods, and deservedly so, since interfaces of lower dimension than the original domain of definition of the partial differential equation are created by a predominant form of nonoverlapping decomposition related to nested dissection of the underlying finite difference or finite element matrix operator. We refer generically to such forms of domain decomposition as Schur iteration, since elimination of the subdomain interiors leaves a Schur complement system for the separator unknowns. Additional interest in interface preconditioning comes from the fact that the classical Schwarz iteration, the prototype for overlapping decompositions, has been placed into correspondence with a stationary iteration having as unknowns the interfacial degrees of freedom of a nonoverlapping decomposition [6, 11]. This correspondence between Schwarz and Schur methods enriches the study of domain decomposition algorithms in general, because properties which are more easily analyzed in one framework may be extended to the other.

The present contribution focuses on the performance of a variety of easily computed Schur complement preconditioners in a rather special context: a single interface dividing a rectangle into two subrectangles in which the capability of performing exact solves is presumed. We consider a scalar convection-diffusion operator under a uniform or "terraced" diffusion coefficient and a variety of continuity-satisfying flow fields chosen to exhibit the relative advantages and disadvantages of the preconditioners. The pristine nature of the problem class allows focusing on the quality of the interfacial preconditioning, alone, in four different limits: large discrete problem size, large Reynolds (or Peclet) number, large diffusion coefficient ratio, and large aspect ratio. (The Reynolds number is the dimensionless ratio $\bar{c}l/\bar{\epsilon}$, where $\bar{c}$ is a characteristic velocity, l a characteristic length, and $\bar{\epsilon}$ a characteristic diffusivity. Large values characterize strongly nonsymmetric, convectively-dominated systems.) Any or all of these limits could be important in a production engineering code whose parallelization might be sought through domain decomposition. We show that no single interface preconditioner is best in all limits, and therefore seek to qualitatively rank their sensitivities to these limits and identify realms of superiority.

Several different coefficient fields $\vec{c}$ and ϵ are studied because the performance of all of the preconditioners are sensitive to them and unjustified optimism or pessimism can result from too narrow a study. Two of our five preconditioners have been amply studied previously in the symmetric positive definite context of pure diffusion. There have been very few studies of any of them in the convection-diffusion context, and since this case is also relatively untouched by theoretical approaches, apart from spatially invariant velocity distributions, numerical studies are continuing to yield interesting information.

We comment briefly on a few other issues which bear on our choice of scope. It is possible to set up an alternative framework for nonoverlapping decompositions in which interfacial coupling is simply discarded, or partially accounted for in ways that do not require special treatment of a separator set; see, *e.g.*, [1] and [26]. In so doing one obtains the advantages of greatly simplified coding and less inter-domain data traffic per iteration. Problems dominated by local interactions can be handled quite acceptably by decoupling; see *e.g.*, [23]. However, in problems which are diffusively dominated (more fundamentally, problems whose Green's functions have support which is not substantially confined within artificial subdomain boundaries), such approaches have limited applicability to large numbers of gridpoints and/or subdomains.

The special case of a single interface obviates discussion of preconditioning the set of vertices where multiple interfaces intersect. Vertex preconditioning is very important but also more readily prescribable, at least in two dimensions. A coarse grid problem for the vertices having the same

structure as the undecomposed original problem can be derived directly from the differential operator by employing a hierarchical basis discretization. The interface system, on the other hand, corresponds to a pseudo-differential operator, the numerical analysis of which is relatively less well developed in the presence of convective terms. In a preconditioner consisting of component blocks corresponding to subdomains, vertices, and interfacial edges (and interfacial planes in three dimensions), any one block can limit the overall performance. A study of interface preconditioning is thus necessary, but not sufficient, for guiding the construction of complete preconditioners.

Finally, as to the relevance of our scope, we note that practical problems often involve several simultaneous convection-diffusion operators linked through coefficients or source terms. Continued study of the scalar case is, however well motivated by techniques such as the alternating block factorization [4] which successfully employ scalar preconditioners *inside* of a change of dependent variables which partially decouples the original system.

The algorithmic framework of our experiments is described in Section 2, followed by introduction of the five interface preconditioners and a brief discussion of their properties in Section 3. Section 4 contains performance measurements in the form of iteration counts along several axes of problem parameter space. We draw some conclusions and recommendations in Section 5.

2. Schur Domain Decomposition Methods

We take as our starting point the matrix equation $Ax = b$ arising from a finite difference discretization of of (1.1). The domain decomposition method we employ is an iterative substructuring method consisting of three elements: (1) the operator A whose inverse action we would like to compute with an accuracy commensurate with the discretization, (2) an approximation B to A, whose inverse action is computationally convenient to compute, and (3) an acceleration scheme for the preconditioned system which requires only the ability to form the actions of A and B^{-1} on a vector. In all cases reported herein, A is derived from a second-order central differencing of the diffusion term and a first-order upwind differencing of the convection term. Extensions to second-order upwind differencing have been carried out in, for instance, [27]. We use right-preconditioned GMRES [30] as our iterative acceleration scheme, that is, we solve $AB^{-1}y = b$ by the applying the standard GMRES algorithm to (AB^{-1}) then recover x through the solution of $Bx = y$.

GMRES is guaranteed to converge in a finite number of steps for nonsingular AB^{-1} even in the presence of nonsymmetry or indefiniteness, assuming exact arithmetic. The maximum number of steps required is the number of distinct eigenvalues of the preconditioned operator. This convergence result depends upon dynamically storing a complete basis for the Krylov space built from powers of AB^{-1} acting on the initial residual vector. For large problems, this much memory can easily become excessive, and GMRES is often truncated or restarted [30] in cases where it does not converge within a predetermined number of steps. However, we allow full GMRES iteration in our experiments, up to some maximum number of steps (set at 30 herein) which is sufficient in all but two cases. Because fewer than 30 steps are almost always sufficient, we effectively suppress from consideration the restart or truncation parameter. This parameter can be important in a "production" setting.

The substructuring enters through the manipulation of A and B into forms which possess large block zeros, for the sake of concurrency or for some of the other reasons noted in the introduction. For elliptic operators such as (1.1), A is irreducible; hence there are no block triangular permutations. However, if the domain is cut by the removal of a swath of gridpoints as wide as the semi-bandwidth of the stencil, two large subproblems are created whose only coupling is through the small removed set. For five-point stencils on logically tensor product grids, we may choose a single row or column of unknowns. (A two-point-wide generalization has been studied for the thirteen-point biharmonic stencil in [8].) Ordering the separators last, we obtain

$$Ax \equiv \begin{pmatrix} A_{11} & 0 & A_{13} \\ 0 & A_{22} & A_{23} \\ A_{31} & A_{32} & A_{33} \end{pmatrix} \begin{pmatrix} x_1 \\ x_2 \\ x_3 \end{pmatrix} = \begin{pmatrix} b_1 \\ b_2 \\ b_3 \end{pmatrix} \equiv b. \tag{2.1}$$

Here, A_{11} and A_{22} are five-point operators with bandwidth no larger than that of the naturally ordered original system, but A_{33}, which renders the coupling between the points on the interface itself, is tridiagonal. The other blocks contain the coupling of the separator unknowns to the subdomains, and vice versa. From the point of view of the continuous operator they represent derivatives in directions normal to the interface.

Block Gaussian elimination of the unknowns x_1 and x_2 would yield the Schur complement system

$$Cx_3 = d \tag{2.2}$$

for x_3, where

$$C = A_{33} - A_{31}A_{11}^{-1}A_{13} - A_{32}A_{22}^{-1}A_{23} \tag{2.3}$$

and

$$d = b_3 - A_{31}A_{11}^{-1}b_1 - A_{32}A_{22}^{-1}b_2. \tag{2.4}$$

If x_3 can be found, the subdomain problems are decoupled. However, direct computation of the generally dense C in order to solve (2.2) requires as many pairs of exact subdomain solves as there are degrees of freedom in x_3, which is generally prohibitive. It is also unnecessary inasmuch as iterative techniques have been devised which require many fewer iterations than the dimension of x_3, and which furthermore require only approximate subdomain solves in each iteration. As mentioned already, we shall ignore the option of inexact subdomain solves in the sequel, effectively reducing the iterations to the interface, but we nevertheless make use of a general purpose code which retains the interior degrees of freedom in carrying out the numerical experiments.

We consider two families of preconditioners B, the structurally symmetric

$$B_1 = \begin{pmatrix} A_{11} & 0 & 0 \\ 0 & A_{22} & 0 \\ A_{31} & A_{32} & M \end{pmatrix} \begin{pmatrix} I & 0 & A_{11}^{-1}A_{13} \\ 0 & I & A_{22}^{-1}A_{23} \\ 0 & 0 & I \end{pmatrix}$$

$$= \begin{pmatrix} A_{11} & 0 & A_{13} \\ 0 & A_{22} & A_{23} \\ A_{31} & A_{32} & M + A_{31}A_{11}^{-1}A_{13} + A_{32}A_{22}^{-1}A_{23} \end{pmatrix},$$

where M approximates the Schur complement C (2.3) of A_{11} and A_{22} in A, and the simpler block triangular

$$B_2 = \begin{pmatrix} A_{11} & 0 & A_{13} \\ 0 & A_{22} & A_{23} \\ 0 & 0 & M \end{pmatrix}.$$

The factorized form of B_1 above shows that the cost of applying the inverse of B_1 is one solve with M and two solves each with A_{11} and A_{22}. There is an inherent sequentiality to the subdomain solves, however, since the system involving M in the left factor requires data from the first set of subdomain solves. The inverse of B_2 can be applied to a vector at the cost of solving one system each with M, A_{11}, and A_{22}. The system for M is solved first, followed by independent solves in the subdomains which use the interface values as boundary conditions.

We assume throughout that the A_{ii} are invertible. (This is certainly a reasonable requirement for a discrete convective-diffusive operator and is guaranteed herein for all Reynolds numbers by upwind differencing.) Under this assumption, C is also invertible [15].

For matrices arising from standard quasi-uniform finite element discretizations of elliptic partial differential equations, A has a condition number of $\mathcal{O}(h^{-2})$, whereas C has a condition number of $\mathcal{O}(h^{-1})$ [5, 29]. The equivalence of conjugate gradient iterations on the Schur complement system with preconditioner M and on the full *substructured* matrix A with preconditioner B_1 was shown in [24].

For reference in Section 4, it is interesting to note the forms of the preconditioned operators AB_1^{-1}, and AB_2^{-1}. In order to make the formulae more readable, we combine the independent subdomain solves into a block matrix A_Ω, and denote the separator block by A_Γ, to re-express the above matrices as

$$A = \begin{pmatrix} A_\Omega & A_{\Omega\Gamma} \\ A_{\Gamma\Omega} & A_\Gamma \end{pmatrix}, \quad B_1 = \begin{pmatrix} A_\Omega & A_{\Omega\Gamma} \\ A_{\Gamma\Omega} & M + A_{\Gamma\Omega}A_\Omega^{-1}A_{\Omega\Gamma} \end{pmatrix}, \quad B_2 = \begin{pmatrix} A_\Omega & A_{\Omega\Gamma} \\ 0 & M \end{pmatrix},$$

whence

$$B_1^{-1} = \begin{pmatrix} A_\Omega^{-1} + A_\Omega^{-1}A_{\Omega\Gamma}M^{-1}A_{\Gamma\Omega}A_\Omega^{-1} & -A_\Omega^{-1}A_{\Omega\Gamma}M^{-1} \\ -M^{-1}A_{\Gamma\Omega}A_\Omega^{-1} & M^{-1} \end{pmatrix}$$

and

$$B_2^{-1} = \begin{pmatrix} A_\Omega^{-1} & -A_\Omega^{-1}A_{\Omega\Gamma}M^{-1} \\ 0 & M^{-1} \end{pmatrix}.$$

From these expressions it can easily be verified that

$$AB_1^{-1} = \begin{pmatrix} I & 0 \\ (I - CM^{-1})A_{\Gamma\Omega}A_\Omega^{-1} & CM^{-1} \end{pmatrix} \text{ and } AB_2^{-1} = \begin{pmatrix} I & 0 \\ A_{\Gamma\Omega}A_\Omega^{-1} & CM^{-1} \end{pmatrix}. \tag{2.5}$$

It is evident that if C is exactly represented by M, then AB_1^{-1} reduces to the identity, and an iteration involving AB_1^{-1} will converge in one step requiring two sets of subdomain solves. An iteration involving AB_2^{-1}, on the other hand, will converge in two steps (from an arbitrary initial guess) if $M = C$, but each step requires only one set of subdomain solves. (These iteration counts do not include the final solve with either B_1 or B_2 which is required to unwind the right-preconditioning.) More generally, if M is sufficiently close to C in the sense that the lower-left block of the structurally symmetric system is small, $||(I - CM^{-1})|| \ll 1$, we expect that an iteration based on B_2 will require an extra iteration relative to an iteration based on B_1. Conversely, if M is a poor preconditioner for C, so that the lower left block becomes large, the use of the structurally symmetric system could require more iterations than the use of the block triangular system. Both behaviors are illustrated in Section 4.

Note from (2.5) that AB_1^{-1} and AB_2^{-1} have identical spectra, as Arnoldi estimates for the eigenvalues obtained as a by-product of the GMRES iterations also show. However, Krylov sequences based on the respective operators will in general differ, and there is little that can be said about which method will lead to faster convergence for general $\vec{c}$ if M and C are not sufficiently close.

For some of the preconditioner components M we consider, the overall preconditioning process is numerical unstable, as will be seen in Section 4. Even though the iterations involving AB^{-1} may converge, the final result after unwinding the preconditioning may have few or even no significant figures. For this reason, we always check the actual residual $||f - Ax||$ at the end of each calculation.

3. Schur Interface Preconditioners

We proceed to delineate five alternatives for the matrix M.

3.1. Interface Probe Preconditioner

Interface probe preconditioning is a family of methods for approximating the true Schur complement C defined in (2.3) by low bandwidth matrices. We use the nomenclature IP(k) to denote

the approximation sequence $M = A_\Gamma - E_k$, $k = 0, 1, 2, \ldots$, where E_k is a matrix of semi-bandwidth k which produces the same action as $A_{\Gamma\Omega}A_\Omega^{-1}A_{\Omega\Gamma}$ on a set of $2k+1$ test vectors. Note that when A arises from a five-point finite-difference discretization both the IP(0) and IP(1) preconditioners are tridiagonal because $A_{\Omega\Gamma}$ is. As k increases beyond 1, M acquires additional diagonals. Selection of test vectors of appropriate sparsity patterns enables the coefficients of E_k to be read directly off of the product involving $A_{\Gamma\Omega}A_\Omega^{-1}A_{\Omega\Gamma}$, hence the term "probe." We report only on the row-sum conserving IP(0) herein. IP(1) is only rarely more cost effective than IP(0) over the range of non-symmetric scalar five-point stencil problems studied herein, and a law of diminishing returns sets in as k is increased.

IP(0) was invented independently by Chan and Eisenstat in 1985, immediately generalized to IP(k) in [14], and adopted for variable coefficient symmetric problems in [24] (where it was called the "modified Schur complement" method) and for nonsymmetric problems in [25, 26]. Symmetric versions of IP(0) and IP(1) have also been employed in [2, 3]. Many algebraic and spectral properties of banded and circulant probe preconditioners are derived in [13]. The interface probe technique has the advantage of being purely algebraic in character, and hence capable of being defined for arbitrary operators. It is aesthetically pleasing that the tunable parameter k may be taken from the crude approximation of 0 all the way to the full bandwidth exact solution. It has also been generalized in a straightforward way to multicomponent systems [26]. However, IP(k) for low k is not expected to be particularly useful for *arbitrary* matrices. The low k limit is motivated by the observation that the elements of C decay rapidly away from the diagonal for elliptic problems. In sufficiently simple elliptic problems (*e.g.*, those possessing constant coefficients) preconditioners described below taking better advantage of this structure are also possible, leaving IP(k) large but not unlimited regions of problem parameter space in which to exercise. Interface probing has the advantage of being automatically adaptive to spatial variation in the coefficients but the disadvantage of not possessing the property of spectral equivalence, a consequence of which is that it degrades as the mesh is refined. Experimentally [24], the condition number of the preconditioned Schur complement system for the Laplacian goes like $h^{-1/2}$, and this bound is conjectured to be the best attainable for any tridiagonal matrix based on experiments with an optimization code in [20]. An $h^{-1/2}$ bound is proved for a circulant probe-preconditioned system with periodic boundary conditions on the boundaries normal to the interface in [13].

3.2. Spectral Preconditioner

The spectral preconditioner is an exact eigendecomposition of a single interface, rectangular domain, constant coefficient convection-diffusion operator described in [12] as a generalization of [7]. We consider only the Dirichlet case herein, but generalizations to Neumann boundary conditions are straightforward. Let an interface of n interior nodes (*i.e.*, $h^{-1} = n+1$) separate two subdomains of the same discrete length, and discrete heights m_1 and m_2, respectively, over all of which is satisfied the difference equation

$$ax_{i-1,j} + bx_{i,j} + cx_{i+1,j} + dx_{i,j+1} + ex_{i,j-1} = f_{i,j}, \tag{3.1}$$

where i denotes the free index *along* the interface. We may write $M = DW\Lambda W^{-1}D^{-1}$, where W is the discrete sine transform of length n with matrix representation

$$[W]_{ij} = \sqrt{2h}\sin ij\pi h, \tag{3.2}$$

D is the diagonal matrix with elements

$$[D]_i = \left(\frac{a}{c}\right)^{(i-1)/2}, \tag{3.3}$$

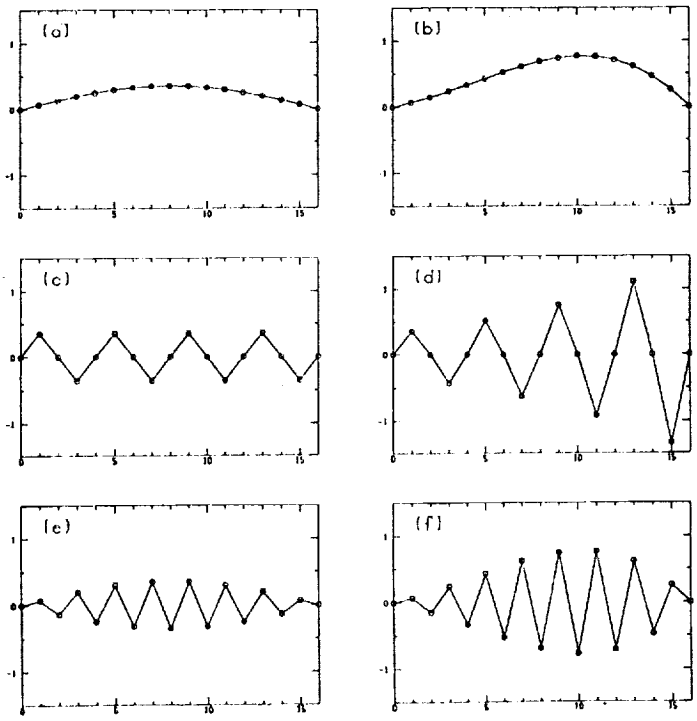

Figure 1: Modes of the Dirichlet problem (3.1) for $n = 15$. (a) $|a/c| = 1$, $j = 1$; (b) $|a/c| = 1.21$, $j = 1$; (c) $|a/c| = 1$, $j = 8$; (d) $|a/c| = 1.21$, $j = 8$; (e) $|a/c| = 1$, $j = 15$; (f) $|a/c| = 1.21$, $j = 15$. (The left-hand column of modes are for the case of no tangential convection.)

and Λ is a diagonal matrix with elements

$$[\Lambda]_i = \frac{1}{2}\left(\frac{1+\gamma_i^{m_1+1}}{1-\gamma_i^{m_1+1}} + \frac{1+\gamma_i^{m_2+1}}{1-\gamma_i^{m_2+1}}\right)\sqrt{[b+\sqrt{ac}(2-\sigma_i)]^2 - 4de}, \tag{3.4}$$

where, in turn,

$$\gamma_i = \frac{1}{4de}\left[b+\sqrt{ac}(2-\sigma_i) + \sqrt{[b+\sqrt{ac}(2-\sigma_i)]^2 - 4de}\right]^2 \tag{3.5}$$

and

$$\sigma_i = 4\sin^2\left(\frac{i\pi}{2(n+1)}\right). \tag{3.6}$$

The derivation of these formulae (see [12] for full details) begins with the observation that the columns of the matrix (DW) are the eigenvectors of the tridiagonal matrix formed by the coefficients along the interface, *viz.*, tridiag(a, b, c). Sample such modes are plotted in Figure 1 for two different values of the ratio $|a/c|$ corresponding to zero and constant nonzero tangential components of the convection. The nonvanishing first-derivative convection term has the effect of multiplying the sinusoids by an exponential.

The philosophy of using the spectral preconditioner for arbitrary interfacial systems is that of solving an approximate (constant coefficient) problem exactly, rather than an exact (general

coefficient) problem approximately. One of its advantages is that it can be defined without requiring the ability to solve problems in adjacent subdomains, as required by the interface probe technique. All that is needed is some averaging rule to obtain the coefficients a through ϵ from the data of the associated regions. All our tests herein employ a simple average of the coefficients along the interface alone. Another advantage is its automatic adaptivity to domain aspect ratio, since the boundary conditions are built into the derivation. We note that application of M^{-1} is inexpensive: two one-dimensional FFTs sandwiched between three diagonal matrix multiplications.

3.3. Spectral Probe Preconditioner

The spectral probe preconditioner, introduced here for the first time, is conceptually a hybrid of the interface probe and the spectral preconditioners. Spectral probing assumes a form for the eigenvectors of C like that derived for the constant coefficient operator of the previous subsection (again based on spatially averaged coefficients), but then populates the diagonal matrix Λ by probing the true Schur complement, so that some spatial adaptivity is accommodated within a spectrally equivalent framework.

We set $M = DW\Lambda W^{-1}D^{-1}$ where W and D are defined as above (or where D is alternatively simply set to the identity matrix, corresponding to $a = c$, for reasons which will become clear in Section 4). Λ is then determined by probing with the interface vector of all 1's. This is the same as the standard test vector for IP(0). To be explicit, we read off the elements of Λ from the equation

$$W^{-1}D^{-1}CDW * \mathbf{1} = \Lambda * \mathbf{1}.$$

The action of C is computed by means of a pair of subdomain solves using $DW * \mathbf{1}$ as the interface boundary condition. Note that the spectral probe preconditioner reduces to the spectral preconditioner in the constant coefficient Dirichlet case, because then C is exactly diagonalized by the given similarity transform.

3.4. Laplacian Square-root Preconditioner

As a base-line reference, and because it appears throughout the literature, we include tests with a method based on the square-root of the one-dimensional Laplacian operator, easily written as:

$$M = W\Lambda W^{-1},$$

where Λ is now the diagonal matrix with elements $[\Lambda]_i = 2\sqrt{\sigma_i}$. We sometimes denote this operator as Dryja's preconditioner because of its popularization in this context in [16]. More general discrete antecedants were considered in [18]. It is difficult to pinpoint the discovery of the spectral equivalence of this operator to the Schur complement of the Laplacian, since the continuous analog of this equivalence has been known for some time. This preconditioner is expected to be good in diffusion-dominated problems, or in the discrete limit $h \to 0$.

Note that this preconditioner is distinct from the spectral preconditioner (§3.2) for the Laplacian. Dryja's preconditioner achieves a constant bound on the number of iterations as the mesh is refined, but the constant is generally higher than that achievable with the coefficient and aspect ratio adaptability of the previous two techniques. The literature also records two important preconditioners intermediate between the Dryja and spectral techniques, namely [19] and [5]. The latter, the Neumann-Dirichlet preconditioner, contains some of the adaptive capabilities of the spectral preconditioner since it relies on subdomain solves in its construction and hence contains much coefficient information. It is similar to probing techniques in this regard. In fact, the Neumann-Dirichlet preconditioner is exact in problems possessing symmetry across the separator set. All four of the techniques of [5, 7, 16, 19] were tested in [24], but for brevity we test only the extremes here.

3.5. Tangential Preconditioner

Finally, we consider a simple preconditioner possessing partial adaptivity, a lower-dimensional restriction of the operator to the interface created by setting all of the normal derivative terms in

the operator to zero and retaining just the remainder in M. For (1.1) these are just the tangential derivative terms. The obvious motivation for this technique is that it is simple and is expected to work well in the limit of strong convection along the interface, a limit which turns out to be troublesome for the spectral and spectral probe preconditioners. In addition, its very satisfactory behavior in the multidomain experiments in [21] recommend it. For reasons not yet theoretically explained, it performs very well in conjunction with the block triangular form of the the overall preconditioner described in Section 2. A minor disadvantage is its requirement of partial knowledge of the differential operator, rather than simply the elements of the discrete operator A. To be specific, it is necessary to store separately the contributions to A arising from the normal derivative terms, and all other terms.

4. Numerical Experiments

All of the experiments to follow except for those of Table 14 are posed on the unit square ($l = 1$ in the definition of the Reynolds number, Re) with homogeneous Dirichlet boundary conditions. The five different continuity-satisfying flow fields tested are shown in Figure 2(b)-(f) , along with a purely diffusive baseline case (Figure 2(a)). When Reynolds numbers are reported below for the variable coefficient cases, they are always based on the maximum velocity in the region. (See [28] for details on the jet and cell flows and other experiments on this particular problem set.) The interface divides the rectangle into equal upper and lower portions, as marked on the figure in the dashed line. In addition to cases with constant diffusion, we study in §4.3 a convectionless case with piecewise constant, but disparate, diffusivities on either side of the interface.

There is a constant source term of unit strength in the interior. Although it is special, a zero initial guess for the solution vector is employed throughout, since this will usually be the natural choice when (1.1) arises for a Newton increment, as part of an outer nonlinear iteration. The performance of the preconditioners is measured by the number of iterations required to reduce the initial residual by a factor of 10^{-5}, regardless of the mesh resolution. The tables of iteration counts are grouped by subsections into four sets of experiments.

4.1. Sensitivity to Mesh Refinement

Tables 1 through 6 examine a constant Re situation as the (uniform) mesh is refined by three successive powers of 2. Of course, the discrete diffusion term, the Laplacian, becomes more and more dominant with each refinement of the grid, since it scales as h^{-2} as compared with the h^{-1} scaling of the convection term. This is the asymptotic limit for which D and its relatives S and SP are designed. In the first table, the Laplacian is studied in isolation (Re = 0). In the next five convective cases, Re = 16. For the coarsest mesh ($h^{-1} = 8$), the contributions to the diagonal of the discrete operator from the two terms are equal at this Reynolds number (the *cell* Reynolds number, $\mathrm{Re}_c \equiv ch/\epsilon$, is 2).

	Structurally Symmetric					Block Triangular				
h^{-1}	IP	S	SP	D	T	IP	S	SP	D	T
8	4	1	1	5	5	5	2	2	4	4
16	6	1	1	5	7	7	2	2	5	4
32	9	1	1	5	9	9	2	2	5	4
64	11	1	1	4	11	12	2	2	5	4

Table 1: Iteration counts for the pure diffusion problem as a function of mesh parameter for two different preconditioner structures and five different interface blocks.

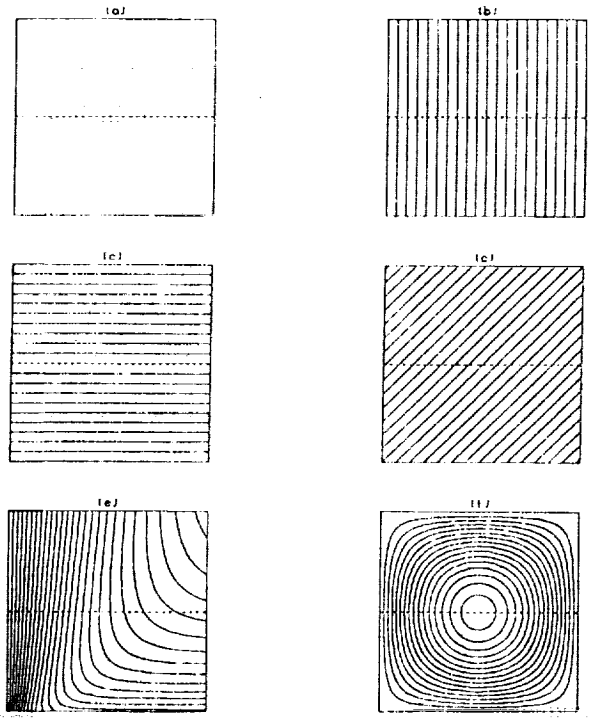

Figure 2: Streamfunction contour plots of the two-dimensional flow fields represented by $\vec{c}$ in the numerical experiments. (a) Pure Diffusion; (b) Normal Convection; (c) Tangential Convection; (d) Skew Convection; (e) Jet Convection (the domain is the right half of a symmetric flow field); (f) Cell Convection.

The S (spectral), SP (spectral probe), and D (Dryja) columns of Table 1 reveal their exactness or spectral equivalence, respectively. Because iteration count is a threshold measurement, most of the data is subject to ± 1 perturbation upon modest adjustment of the convergence tolerances, but the S and SP residuals at convergence are zero to machine precision. The deterioration of IP like some negative power of h is evident on both the structurally symmetric (B_1) and block triangular (B_2) sides of the table. The tangential preconditioner is the only one with markedly different performance depending upon the structure of B. Here, as below, it is excellent in conjunction with the block triangular form.

	Structurally Symmetric					Block Triangular				
h^{-1}	IP	S	SP	D	T	IP	S	SP	D	T
8	3	1	1	4	5	4	2	2	4	5
16	5	1	1	5	7	6	2	2	5	5
32	6	1	1	5	9	7	2	2	5	5
64	7	1	1	5	12	8	2	2	5	5

Table 2: Same as Table 1, except for normal convection at a Reynolds number of 16.

Table 2, for a normal convection problem, is similar to Table 1 except that IP improves slightly

as each of the terms $A_{31}A_{11}^{-1}A_{13}$ and $A_{32}A_{22}^{-1}A_{23}$ being approximated by a diagonal matrix becomes less important relative to A_{33} because one of the coupling matrices is small. For instance, if the convection is from subdomain 1 into subdomain 2, A_{13} and A_{32} are weak.

	Structurally Symmetric					Block Triangular				
h^{-1}	IP	S	SP	D	T	IP	S	SP	D	T
8	5	1	7	8	6	5	2	8	7	4
16	6	1	10	10	9	7	2	11	10	5
32	8	1	11	11	11	9	2	12	11	5
64	11	1	12	11	15	12	2	13	11	5

Table 3: Same as Table 1, except for tangential convection at a Reynolds number of 16.

The importance of the D matrix in the spectral preconditioner is evident in Table 3 in which a tangential convection problem is considered. The version of SP employed in this study approximates the D in its definition as the identity; using the true D here would reproduce the spectral results in this constant coefficient case, just as in the previous two tables in which $D = I$ anyway. Though SP and D are spectrally equivalent, they require an order of magnitude more iterations than S, and are surpassed by IP in the smaller problem range on the structurally symmetric side, and by the tangential preconditioner on the block triangular side.

	Structurally Symmetric					Block Triangular				
h^{-1}	IP	S	SP	D	T	IP	S	SP	D	T
8	4	1	7	8	7	5	2	8	8	6
16	5	1	9	10	9	6	2	10	9	6
32	7	1	10	10	12	8	2	11	10	6
64	9	1	10	10	15	10	2	11	11	7

Table 4: Same as Table 1, except for skew convection at a Reynolds number of 16.

Table 4 contains the last of the constant coefficient test examples, featuring a skew convection (inclined at 45 degrees relative to the interface). Overall results are not very different from the purely tangential convection case. Most of the entries in the skew table lie at or between corresponding entries in the normal and tangential tables. Those of the tangential preconditioner, however, are often worse in the intermediate skew convection case than at either extreme.

	Structurally Symmetric					Block Triangular				
h^{-1}	IP	S	SP	D	T	IP	S	SP	D	T
8	5	4	5	6	6	5	5	6	6	5
16	6	4	6	6	8	7	5	7	7	6
32	9	4	6	6	11	10	5	7	7	7
64	11	4	6	6	14	12	5	7	7	8

Table 5: Same as Table 1, except for jet convection at a Reynolds number of 16.

The jet case recorded in Table 5 tends to level the preconditioner landscape because the constant coefficient approximation of S is no longer exact. S remains the best technique as h^{-1} increases, but its margin of superiority over other spectrally equivalent techniques (with D as a nonadaptive extreme) is small.

	Structurally Symmetric					Block Triangular				
h^{-1}	IP	S	SP	D	T	IP	S	SP	D	T
8	4	5	4	5	5	5	5	5	5	5
16	6	5	5	6	7	7	6	6	6	6
32	9	5	5	5	9	10	6	6	6	6
64	11	5	5	5	11	12	6	6	6	6

Table 6: Same as Table 1, except for cell convection at a Reynolds number of 16.

The cell case of Table 6 is the greatest equalizer among the test cases, because the interface cuts a zone of recirculation, *i.e.*, there is normal flow across it in both directions, and none of the methods holds an edge of superiority. Performance under the block tridiagonal preconditioner is notably uniform for the last four methods.

4.2. Sensitivity to Reynolds Number

Tables 7 through 11 examine the influence of increasing Reynolds number. Values of Re of 0, 4, 16, 64, 256, and 1024 are considered at $h^{-1} = 64$. Thus, the third row of each table in this subsection is the same as the last row of the table of corresponding flow type in the first set, and the first row of each table is the same as the last row of the pure diffusion case in Table 1. Progressing down the rows of the table the nonsymmetry of the operator increases. Between rows four and five the convection terms begin to contribute more heavily than the diffusion terms to the diagonal elements of A.

	Structurally Symmetric					Block Triangular				
Re	IP	S	SP	D	T	IP	S	SP	D	T
0	11	1	1	4	11	12	2	2	5	4
4	10	1	1	4	11	11	2	2	5	4
16	7	1	1	5	12	8	2	2	5	5
64	5	1	1	7	14	6	2	2	7	6
256	3	1	1	11	17	4	2	2	10	9
1024	2	1	1	15	22	3	2	2	12	16

Table 7: Iteration counts for the normal convection problem at a constant mesh parameter of 1/64 as a function of Reynolds number for two different preconditioner structures and five different interface blocks.

Table 7 shows that in the presence of constant normal convection, techniques S and SP remain exact at any Re, while IP catches up at high Re, and D and T successively worsen. (For D, this is the drawback of finite h in a method derived for $h \to 0$.) Qualitatively, the trends are the same for either preconditioner structure, although the tangential method continues to be much better in the block triangular formulation.

The Achilles' heel of the spectral technique appears when there is strong convection tangential to the interface, as seen in Table 8. In this limit in which $|a/c|$ differs sufficiently from unity the

	Structurally Symmetric					Block Triangular				
Re	IP	S	SP	D	T	IP	S	SP	D	T
0	11	1	1	4	11	12	2	2	5	4
4	12	1	7	7	14	13	2	8	8	5
16	11	1	12	11	15	12	2	13	11	5
64	8	1	20	15	14	9	2	21	15	3
256	7	-	>	20	12	8	-	>	19	1
1024	5	-	>	26	8	6	-	>	24	1

Table 8: Same as Table 7, except for tangential convection. The hyphen denotes loss of precision, and the ">" more than 30 iterations.

latter terms in D, which have this ratio raised to as much as $(n-1)^{st}$ power, can approach the machine epsilon (or its reciprocal, depending upon the direction of the convection). In reference to (3.3), we note that for $n = 64$, $(a/c)^{(n-1)/2} \approx \epsilon_{\text{mach}} \approx 10^{-16}$ when $(a/c) \approx 10^{(-32/63)} \approx 0.31$. Under upwind differencing, it only takes a cell Reynolds number of 2 to produce a ratio of 3 between the upwind and downwind stencil coefficients a and c. Thus, $\text{Re}_c = 2$ is the borderline of stability for the spectral preconditioner with respect to tangential convection. In the tables, the Re = 64 row corresponds to a cell Reynolds number of unity, and the Re = 256 row to a cell Reynolds number of 4; thus, they straddle the transition. GMRES iterations based on the spectral interface preconditioner do terminate for the hyphenated entries, but the residuals based on the resulting x vectors shows complete loss of precision.

The spectral probe technique does not lose precision, because of the assumption that $D = I$; however, a diagonal approximation for $W^{-1}CW$ is poor, and it simply takes too long to converge. The Dryja preconditioner, which makes no attempt to adapt to the strong directionality of the problem also deteriorates with Re. At low Re where M and C are close, the B_1 iteration count is lower by one; but at high Re, where isotropic M is very different from unidirectional C, the B_2 iteration count is better. The interface probe technique meanwhile improves with Re as it captures more of the increasingly diagonally dominant problem within its own sparsity structure. Finally, the tangential technique is excellent for a tangentially dominated operator. The cross-diffusion which it neglects becomes of negligible importance as the problem effectively decouples into independent problems for A_{11}, A_{22}, and A_{33} in which the upstream boundary condition is all important.

	Structurally Symmetric					Block Triangular				
Re	IP	S	SP	D	T	IP	S	SP	D	T
0	11	1	1	4	11	12	2	2	5	4
4	11	1	7	7	14	12	2	8	8	6
16	9	1	10	10	15	10	2	11	11	7
64	7	1	13	14	17	7	2	14	14	8
256	4	-	13	18	19	5	-	14	16	9
1024	3	-	13	20	19	4	-	15	17	10

Table 9: Same as Table 7, except for skew convection.

Most of the observations of the high Re tangential flow also apply to the skew flow in Table 9, however, the latter differentiates between IP, which repeats its tendency to improve as Re grows, and T, which no longer matches the physics of the problem, and is worse than IP, although it is still superior to the Fourier-based methods as a module of the block triangular preconditioner.

We also note that the spectral probe technique captures a significant part of the physics in this case, adapting to the co-dominant normal convection and tending to a constant iteration count without breaking down. It thus rescues the spectral technique and indicates how the robustness of the spectral preconditioner can be maintained with a compromise in efficiency. In a general purpose code, the elements of the D matrix could differ from unity but be bounded artificially, allowing partial tangential adaptivity with full normal adaptivity.

	Structurally Symmetric					Block Triangular				
Re	IP	S	SP	D	T	IP	S	SP	D	T
0	11	1	1	4	11	12	2	2	5	4
4	11	3	4	5	14	12	4	5	6	6
16	11	4	6	6	14	12	5	7	7	8
64	10	6	9	9	14	11	7	10	10	9
256	9	7	11	14	13	10	8	12	14	10
1024	9	–	20	19	14	10	–	21	18	11

Table 10: Same as Table 7, except for jet convection.

As in the spectral equivalence tests in Table 5, the jet case recorded in Table 10 tends to diminish the extremes of preconditioner behavior relative to the uniform skew convection case. The IP and SP results worsen while the D and T methods nearly hold their own relative to Table 9. The pure spectral method survives at a higher overall Reynolds number because the tangential velocities at the interface are lower than the maximum core velocity of the jet, to which Re is scaled.

	Structurally Symmetric					Block Triangular				
Re	IP	S	SP	D	T	IP	S	SP	D	T
0	11	1	1	4	11	12	2	2	5	4
4	11	3	3	4	11	12	4	4	5	5
16	11	5	5	5	11	12	6	6	6	6
64	13	8	7	8	13	14	9	8	9	8
256	18	14	11	14	16	19	15	12	14	15
1024	25	23	16	23	26	26	23	17	23	24

Table 11: Same as Table 7, except for cell convection.

Again, the cell case of Table 11 is an equalizer for most of the methods; however, the performance of the spectral probe technique is singularly good. This is easily explained as follows: the average tangential velocity along the interface is zero because of the symmetry of Figure 2(f), so $D = I$ for both S and SP. However, S also employs an zero average for the normal velocity, whereas SP adapts to strong inflow and outflow along opposite halves of the interface. The performance of IP, which improves with Re in all previous tables, deteriorates in this table because no pair of coupling matrices is weak (see comments on Table 2) under recirculation. Performances under the structurally symmetric and block tridiagonal schemes of the tangential preconditioner become similar at high Re. The recirculating cell flow is in some sense a worst case for a single interface. If the domain of Figure 2(f) is further decomposed by a vertical interface, putting a vertex in the center, all four interfaces would be free of two-signed velocity components, and easier to precondition. (The cross-point preconditioning then becomes an important subject.)

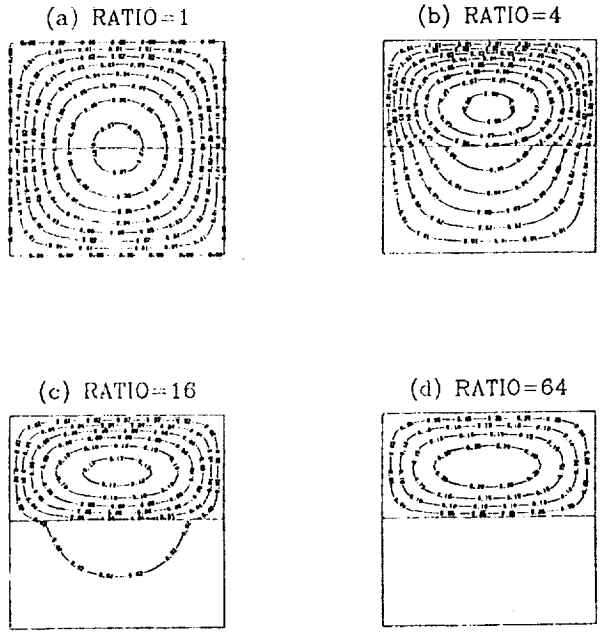

Figure 3: Contour plots of the solution to $\nabla \cdot \epsilon \nabla u = f$ with homogeneous Dirichlet boundary conditions and $f = 1$ for various ratios of the (piecewise constant) diffusivity in the adjoining subdomains. "Ratio" is $\epsilon_{lower}/\epsilon_{upper}$ and the product $\epsilon_{lower}\epsilon_{upper}$ is maintained at unity.

4.3. Piecewise Constant Diffusivity

This subsection focuses on the effectiveness of the preconditioners in heterogeneous problems. With reference to Figure 3, we assign a higher diffusivity in the lower domain than in the upper. We report convergence results in two limits: fixed diffusivity ratio and increasing h^{-1} (Table 12) and fixed h^{-1} and increasing diffusivity ratio (Table 13).

The performance of the two probe and the tangential preconditioners in the terraced diffusivity case in Table 12 is identical to their performance in the uniform case of Table 1. However, the Dryja preconditioner is slightly worse and the spectral preconditioner (based on the arithmetically averaged diffusivity) is much worse than in the uniform case. In fact, S is the worst preconditioner in the terraced diffusion case while SP is the best, the probe supplying crucial information.

As the ratio of diffusivities increases for a fixed problem size, as in Table 13, all methods asymptote monotonically to fixed convergence rates, as shown theoretically in [13]. The physical interpretation of the asymptotically large diffusivity ratio is that virtually all of the variation of solution in response to the (fixed) forcing occurs in the subdomain with the lesser diffusivity. Figure 3 illustrates this phenomenon. The contours are kinked at the interface since it is the normal component of the diffusive flux, $\epsilon \nabla u$, not ∇u itself, which must balance on either side. The solution along the interface is asymptotically the boundary value of zero. The spectral probe method is a singularly good performer in this limit.

4.4. Sensitivity to Aspect Ratio

Table 14 examines the constant diffusion case under aspect ratios ranging from $1{:}\frac{1}{16}$ (a squat

	Structurally Symmetric					Block Triangular				
h^{-1}	IP	S	SP	D	T	IP	S	SP	D	T
8	4	4	1	5	5	5	5	2	5	4
16	6	6	1	5	7	7	7	2	5	4
32	9	9	1	6	9	9	9	2	5	4
64	11	12	1	6	11	12	13	2	5	4

Table 12: Iteration counts for the step diffusion problem as a function of mesh parameter for two different preconditioner structures and five different interface blocks. The ratio of the diffusion coefficients of the two subdomains is 64.

	Structurally Symmetric					Block Triangular				
Ratio	IP	S	SP	D	T	IP	S	SP	D	T
1	9	1	1	5	9	9	2	2	5	4
4	9	7	1	5	9	9	8	2	5	4
16	9	8	1	5	9	9	9	2	5	4
64	9	9	1	6	9	9	9	2	5	4
256	9	9	1	6	9	9	9	2	6	4
1024	9	9	1	6	9	9	9	2	6	4

Table 13: Iteration counts for the step diffusion problem at a constant mesh parameter of 1/32 as a function of diffusivity ratio for two different preconditioner structures and five different interface blocks.

rectangle with subdomains just two cells high) to 1:2 (a tall rectangle composed of two square subdomains). Note that the discrete length of the interface, n, remains constant at 63 in all examples, while heights m_1 and m_2 vary from 1 to 63.

	Structurally Symmetric					Block Triangular				
(l_x, l_y)	IP	S	SP	D	T	IP	S	SP	D	T
$(1, \frac{1}{16})$	4	1	1	8	14	4	2	2	8	13
$(1, \frac{1}{8})$	5	1	1	6	13	6	2	2	6	10
$(1, \frac{1}{4})$	7	1	1	5	12	8	2	2	5	7
$(1, \frac{1}{2})$	9	1	1	5	11	10	2	2	5	5
$(1, 1)$	11	1	1	4	11	12	2	2	5	4
$(1, 2)$	9	1	1	4	8	10	2	2	5	2

Table 14: Iteration counts for the pure diffusion problem at a constant mesh parameter of 1/64 as a function of aspect ratio for two different preconditioner structures and five different interface blocks.

We confirm that S and SP are completely adaptive to aspect ratio in this constant coefficient problem, which is not true of any other method, including Dryja's. The tangential preconditioner is understandably good when the narrow (more strongly boundary influenced) direction is the tangential one, and poorer when this aspect ratio is reversed. The nonmonotonic character of IP is interesting, showing that it adapts well to either extreme and is poorest in the balanced

intermediate case.

5. Conclusions

We conclude by pulling together some overall assessments of the preconditioners tested in the previous section. The interface probe technique is the most general purpose and robust of the methods. It is always definable and adapts well to high Re and extreme aspect ratio, but is nonoptimal at high h^{-1} and is occasionally the worst method. It does very well in predominantly unidirectional strongly convective flows. Generalizations to multiple interfaces, multiple components, and inexact subdomain solves are straightforward, but not pursued herein (see [26]).

The spectral method is mathematically the method of choice asymptotically in h^{-1}, where physically well resolved problems should end up. However, since it is based on a global constant-coefficient approximation it does not perform well in heterogeneous problems. Furthermore, high cell Reynolds numbers can cause it to go unstable, and flow fields whose actual values along the interface differ greatly from their average values are poorly represented. A stabilizing technique was proposed which could preserve the robustness of the spectral method at high cell Reynolds numbers, namely selection of an exponent base for D in (3.3) closer to unity than the true $|a/c|$.

The spectral probe method is as good as the spectral method when W alone is a good approximation to the eigenvectors of C (*i.e.*, low tangential convection). A D-modulated version of spectral probe can be just as effective (and just as vulnerable to strong tangential convection) as the pure spectral method in a constant coefficient problem. SP adapts better than S to normal convection variation and it adapts perfectly to piecewise constant heterogeneities in the diffusivity. As a "probe" method, it shares the coding disadvantages of IP.

The Dryja preconditioner is never exclusively the best method, but is as good as either S or SP in a variable coefficient problem in the limit $h \to 0$, where the diffusive contributions to A dominate. However, the extra cost of S is insignificant compared to D, and SP costs only extra subdomain solves in the pre-processing, so these techniques (suitably stabilized for tangential convection) will almost always be preferable in applications.

All of the above techniques are relatively insensitive to the choice of the overall preconditioner structure. The tangential interface preconditioner is an exception, for reasons yet to be explained theoretically. It is much better under the block triangular form of the overall preconditioner, and is very competitive with the other techniques under physically predictable circumstances, namely tangentially dominant convection or narrow aspect ratio. It is also simple to code and has been successfully generalized to multicomponent systems (see [22]).

We note that when exact subdomain solves are performed, the block triangular form of the preconditioner, B_2, with its one-directional flow of information from the separators to the interiors, is almost always preferable to the structurally symmetric form B_1 in terms of execution time, since a full set of subdomain solves is saved at each iteration and the iteration counts are usually comparable. The structurally symmetric form is also obviously useful when A is itself symmetric, since it then admits preconditioned conjugate gradients rather than GMRES as the iterative solver.

Clearly, a user who understands his problem physically and is willing to customize can do well by choosing among a variety of interface preconditioner modules, perhaps using different ones on differently resolved grids within the same overall solution procedure. Hopes of finding a single "best" method from among those considered must clearly be dismissed, but the field is still young. It is clear that general purpose adaptivity will require some form of "probing" via subdomain solves; taken to the limit, one obtains C directly. Such probing has an associated cost comparable to an iteration step, and must be undertaken conservatively. Future developments which iteratively improve the interface preconditioning based on accumulated subdomain solve data would be welcome, and so would more hybrids along the lines of the spectral probe which incorporate both analytical and numerical data.

References

[1] C. Ashcraft, *Domain Decoupled Incomplete Factorizations,* Technical Report ETA-TR-49, Boeing Computer Services, April 1987.

[2] O. Axelsson & B. Polman, *Block Preconditioning and Domain Decomposition Methods, I,* Technical Report 8735, Dept. of Mathematics, Catholic University, Nijmegen, December 1987.

[3] ———, *Block Preconditioning and Domain Decomposition Methods, II,* J. Comp. Appl. Math., 24 (1988), pp. 55–72.

[4] R. E. Bank, T. F. Chan, W. M. Coughran, Jr. & R. K. Smith, *The Alternate-Block-Factorization Procedure for Systems of Partial Differential Equations,* Technical Report Numerical Analysis Manuscript 89-5, AT& Bell Laboratories, July 1989.

[5] P. E. Bjorstad & O. B. Widlund, *Iterative Methods for the Solution of Elliptic Problems on Regions Partitioned into Substructures,* SIAM J. Num. Anal., 23 (1986), pp. 1097–1120.

[6] ———, *To Overlap or Not to Overlap: A Note on a Domain Decomposition Method for Elliptic Problems,* SIAM J. Sci. Stat. Comp., 10 (1989), pp. 1053–1061.

[7] T. F. Chan, *Analysis of Preconditioners for Domain Decomposition,* SIAM J. Num. Anal., 24 (1987), pp. 382–390.

[8] ———, Boundary Probe Preconditioners for Fourth Order Elliptic Problems, T. F. Chan, R. Glowinski, J. Periaux & O. Widlund ed., *Second International Symposium on Domain Decomposition Methods,* SIAM, Philadelphia, 1989, pp. 160–167.

[9] T. F. Chan, R. Glowinski, J. Periaux & O. Widlund, *Second International Symposium on Domain Decomposition Methods,* SIAM, Philadelphia, 1989.

[10] ———, *Third International Symposium on Domain Decomposition Methods for Partial Differential Equations,* SIAM, Philadelphia, 1990.

[11] T. F. Chan & D. Goovaerts, *Schwarz = Schur: Overlapping versus Nonoverlapping Domain Decomposition,* Technical Report 88-21, UCLA Comp. and App. Math., August 1988. (To appear in SIAM J. Matrix Anal. and Appl.).

[12] T. F. Chan & T. Y. Hou, *Domain Decomposition Preconditioners for General Second Order Elliptic Operators,* Technical Report 88-16, UCLA Comp. and App. Math., June 1988.

[13] T. F. Chan & T. P. Mathew, *The Boundary Probing Technique in Domain Decomposition,* Technical Report 91-02, UCLA Comp. and App. Math., February 1991.

[14] T. F. Chan & D. Resasco, *A Survey of Preconditioners for Domain Decomposition,* Technical Report 414, Computer Science Dept., Yale University, September 1985. (In Proceedings of the IV Coloquio de Matemáticas del CINVESTAV, Workshop in Numerical Analysis and its applications, Taxco, Mexico, Aug. 18-24, 1985).

[15] R. W. Cottle, *Manifestations of the Schur Complement,* Lin. Alg. Appl., 8 (1974), pp. 189–211.

[16] M. Dryja, *A Capacitance Matrix Method for Dirichlet Problem on Polygonal Region,* Numer. Math., 39 (1982), pp. 51–64.

[17] R. Glowinski, G. H. Golub, G. A. Meurant & J. Periaux, *First International Symposium on Domain Decomposition Methods for Partial Differential Equations,* SIAM, Philadelphia, 1988.

[18] R. Glowinski & O. Pironneau, *Numerical Methods for the First Biharmonic Equation and for the Two-Dimensional Stokes Problem,* SIAM Review, 21 (1979), pp. 167–212.

[19] G. H. Golub & D. Mayers, The Use of Preconditioning over Irregular Regions, R. Glowinski & J. L. Lions ed., *Computing Methods in Applied Sciences and Engineering VI,* North Holland, 1984, pp. 3–14.

[20] A. Greenbaum & G. Rodrigue, *Optimal Preconditioners of a Given Sparsity Pattern,* Technical Report 431, Courant Institute, February 1989.

[21] W. D. Gropp & D. E. Keyes, *Domain Decomposition with Local Mesh Refinement,* Technical Report 91-20, Inst. for Comput. Appl. Sci. Eng., January 1991. (to appear in SIAM J. Sci. Stat. Comp.).

[22] ———, *Domain Decomposition Methods in Computational Fluid Dynamics,* Technical Report 91-20, Inst. for Comput. Appl. Sci. Eng., January 1991. (to appear in Int. J. Num. Meths. Fluids).

[23] D. E. Keyes, *Domain Decomposition Methods for the Parallel Computation of Reacting Flows,* Comput. Phys. Comm., 53 (1989), pp. 181–200.

[24] D. E. Keyes & W. D. Gropp, *A Comparison of Domain Decomposition Techniques for Elliptic Partial Differential Equations and their Parallel Implementation,* SIAM J. Sci. Stat. Comp., 8 (1987), pp. s166-s202.

[25] ———, Domain Decomposition for Nonsymmetric Systems of Equations: Examples from Computational Fluid Dynamics, T. F. Chan, R. Glowinski, J. Periaux & O. Widlund ed., *Second International Symposium on Domain Decomposition Methods,* SIAM, Philadelphia, 1989, pp. 321–339.

[26] ———, *Domain Decomposition Techniques for the Parallel Solution of Nonsymmetric Systems of Elliptic BVPs,* Appl. Num. Math., 6 (1990), pp. 281–301.

[27] ———, *Domain-Decomposable Preconditioners for Second-order Upwind Discretizations of Multicomponent Systems,* Technical Report MCS-P187-1090, Argonne National Laboratory, November 1990.

[28] D. E. Keyes, W. D. Gropp & A. Ecder, Domain Decomposition Techniques for Large Sparse Nonsymmetric Systems Arising from Elliptic Problems with First-Order Terms, J. H. Kane & A. D. Carlson ed., *Proceedings of a Symposium on the Solution of Super Large Problems in Computational Mechanics,* Plenum, New York, 1989, pp. 251–266.

[29] L. Mansfield, *On the Conjugate Gradient Solution of the Schur Complement System Obtained from Domain Decomposition,* SIAM J. Num. Anal., 27 (1990), pp. 1612–1620.

[30] Y. Saad & M. H. Schultz, *GMRES: A Generalized Minimum Residual Algorithm for Solving Nonsymmetric Linear Systems,* SIAM J. Sci. Stat. Comp., 7 (1986), pp. 856–869.

Layer tracking, asymptotics, and domain decomposition

by
D. L. Brown
Computing and Communications Div., LANL, Los Alamos, NM 87545
R. C. Y. Chin
Computer Science, IUPUI, Indianapolis, IN 46205
G. W. Hedstrom
LLNL, L-321, P. O. Box 808, Livermore, CA 94550
T. A. Manteuffel
University of Colorado Denver, Denver, CO 80202

Abstract

In this paper we present a preliminary report on our work on the tracking of internal layers in a singularly-perturbed convection-diffusion equation. We show why such tracking may be desirable, and we also show how to do it using domain decomposition based on asymptotic analysis.

1 Introduction

In this paper we present the analogue of a shock-tracking scheme for the resolution of an internal layer and its interaction with an ordinary boundary layer at the outflow. In the computation of compressible flows at high Mach number there has long been competition between shock tracking and shock capturing, and it is now generally agreed that both are needed. We generally find that the number of strong shocks is small, and they should be tracked in order to assure accuracy of the solution. For reasons of efficiency, however, the large number of weak shocks reverberating around the domain should be computed by a reliable shock-capturing scheme such as Roe's method [14] or the method of Colella and Woodward [7]. Shocks are not always the most important features in fluid flows, but the tracking of such other phenomena is still far behind shock tracking. We first show why it may be desirable to track an internal layer, and then we show how such tracking may be accomplished via domain decomposition.

For the sake of simplicity we consider a specific time-independent, singularly-perturbed, convection-diffusion equation

$$a\,\partial_x u + b\,\partial_y u = \epsilon\,\Delta u + F \tag{1.1}$$

on a bounded domain Ω in the (x,y)-plane. Here, Δ denotes the Laplace operator, and ϵ is a small, positive number. For the moment, we impose Dirichlet conditions $u = f$ on the boundary $\partial\Omega$, but later we sometimes treat mixed boundary conditions. The function f is required to be piecewise smooth. (We use the term 'smooth' to mean some convenient degree of differentiability, say C^2.) We assume that the coefficients a and b are smooth functions of x and y on Ω. The source term F is assumed to be a smooth function of x, y, and u. Furthermore, we impose the restriction that $|a| + |b| \neq 0$ in the closure of Ω. This assumption implies that there are no stagnation points, and it greatly diminishes the complexity of the domain decomposition. Our assumption of semilinearity is much less restrictive because nonlinear problems are often solved via a sequence of linear problems with variable coefficients. Our discussion does not pertain to shock layers, however, since they violate the assumption of smoothness of a and b.

Previous work [4], [11], [12] on algorithms for (1.1) using domain decomposition based on asymptotic analysis has treated the special case of $b = 0$. It is true that a transformation of coordinates may be used to convert (1.1) to the case $b = 0$. In this paper we show why such a transformation is very desirable, and we present an algorithm to carry it out.

The development of numerical methods for (1.1) in the singularly-perturbed case requires an understanding of the asymptotic behavior of its solutions as $\epsilon \downarrow 0$. We therefore begin with a brief description of the relationship between u and the solution U of the reduced equation

$$a\,\partial_x U + b\,\partial_y U = F. \tag{1.2}$$

For more details see the books by Chang and Howes [1] and Eckhaus [8]. Equation (1.2) is easily solved by the method of characteristics,

$$\frac{dx}{ds} = a, \qquad \frac{dy}{ds} = b, \qquad \frac{dU}{ds} = F. \tag{1.3}$$

The first two equations in (1.3) define characteristic curves. It is clear that we cannot impose the boundary condition $U = f$ at every intersection of a characteristic curve with $\partial\Omega$. Instead, we subdivide $\partial\Omega$ into three sets, depending on the direction of the vector (a,b). The *inflow boundary* Γ_I is the subset of $\partial\Omega$ on which (a,b) points into Ω, the *outflow boundary* Γ_O is the subset of $\partial\Omega$ on which (a,b) points out of Ω, and the *tangential boundary* Γ_T is the subset of $\partial\Omega$ on which (a,b) is tangent to $\partial\Omega$. For (1.3) the boundary condition $U = f$ is imposed only on the inflow boundary Γ_I.

It is reasonable to expect to have $u \approx U$ for the solutions u of (1.1) wherever Δu is not too large, i.e, wherever u is smooth. Because of the smoothness of the source term F and of the coefficients a and b, the only mechanism for introducing nonsmooth behavior into the solution u of (1.1) is through the boundary condition $u = f$. One obvious difficulty is that we cannot force $U = f$ on the outflow and tangential boundaries $\Gamma_O \cup \Gamma_T$. The resolution of this difficulty is that there are boundary layers across which u changes rapidly from $u \approx U$ to $u = f$. More precisely, when f is smooth the relation $u \approx U$ is true except in the following

portions of Ω. There may be what are called *parabolic boundary layers* along the tangential boundary Γ_T, and there may be *ordinary boundary layers* along the outflow boundary Γ_O.

Let us take a moment to explain the terminology 'ordinary boundary layer' and to describe its properties. Consider a point P on Γ_O. In the vicinity of P we may construct a transformation $(\sigma, \tau) \mapsto (x, y)$ such that the origin $(\sigma, \tau) = (0, 0)$ is mapped to the point P. We may further require that the portion of a neighborhood of the origin with $\sigma > 0$ is mapped into Ω, so that a segment of the axis $\sigma = 0$ is mapped onto a segment of the boundary Γ_O. In terms of the variables σ and τ the differential equation (1.1) takes the form

$$\widehat{a}\,\partial_\sigma u + \widehat{b}\,\partial_\tau u = \epsilon(c_1\,\partial_\sigma^2 u + c_2\,\partial_\sigma\partial_\tau u + c_3\,\partial_\tau^2 u) + F. \tag{1.4}$$

Note that the definition of outflow boundary implies that if c_1 is chosen to be positive, then it follows that $\widehat{a} < 0$. We have seen that we expect to have $u \approx U$ away from the boundary $\sigma = 0$, while we require that $u = f$ on the boundary $\sigma = 0$. That is, we expect u to vary slowly with respect to τ but rapidly with respect to σ. Let us therefore introduce the scaling

$$\sigma = \epsilon\widehat{\sigma}, \qquad \tau = \widehat{\tau} \tag{1.5}$$

into (1.4). If we formally discard all but terms of the order of $1/\epsilon$, we obtain a reduced equation

$$\widehat{a}\,\partial_{\widehat{\sigma}} V = c_1\,\partial_{\widehat{\sigma}}^2 V. \tag{1.6}$$

The term ordinary boundary layer derives from the fact that (1.6) is an ordinary differential equation. The term exponential boundary layer is also used, because the solution V of (1.6) is the sum of a constant and an exponential function. Note that because $\widehat{a}/c_1 < 0$, this exponential decreases with increasing $\widehat{\sigma}$. Note also that in terms of the variable σ the rate of decrease is of the order of $\exp\{-\kappa\sigma/\epsilon\}$, where κ is an average value of $|\widehat{a}|/c_1$. We therefore expect the width of the ordinary boundary layer to be $O(\epsilon)$. The book by Chang and Howes [1] gives theoretical justification for all of these heuristic manipulations.

In the vicinity of the tangential boundary Γ_T we use the characteristic curves (1.3) to define one set of coordinate lines, and we use them as the foundation for a local mapping $(s, t) \mapsto (x, y)$ in the vicinity of a point P on Γ_T. In terms of these coordinates (1.1) takes the form

$$\partial_s u = \epsilon(c_4\,\partial_t^2 u + c_5\,\partial_s\partial_t u + c_6\,\partial_t^2 u) + F. \tag{1.7}$$

We remark that the definition of flow direction implies that $c_6 > 0$. We may require that a segment of the axis $t = 0$ maps onto a segment of the boundary Γ_T and that positive values of t correspond to points in the interior of Ω. Thus, the boundary layer has to accommodate a rapid transition from $u \approx U$ for $t > 0$ to $u = f$ at $t = 0$. Let us therefore introduce the scaling

$$s = \widehat{s}, \qquad t = \widehat{t}\sqrt{\epsilon} \tag{1.8}$$

into (1.7). If we formally delete all terms smaller than $O(1)$, we obtain the reduced equation

$$\partial_{\widehat{s}} W = c_4\,\partial_{\widehat{t}}^2 W + F. \tag{1.9}$$

This equation is parabolic, giving rise to the term parabolic boundary layer. Furthermore, the thickness of the boundary layer for (1.9) is $O(1)$ with respect to $\hat{t}$. With respect to t the parabolic boundary layer is therefore of width $O(\sqrt{\epsilon})$. Again, theoretical justification for these remarks may be found in [1].

If f has a discontinuity at a point P on Γ_I, then by (1.3) the function U will have a corresponding discontinuity in Ω along the characteristic curve γ through P. Similarly, if the Lie derivative of f along Γ_I is discontinuous at P, then grad U is discontinuous along γ. Because u is smooth, the lack of smoothness of U causes u to deviate substantially from U in a neighborhood of γ. As in the case of a parabolic boundary layer, if we introduce coordinates (s,t) derived from the characteristic variable s as given by (1.3), we find that (1.1) maps to an equation of the form (1.7) and that (1.9) is the appropriate reduced equation. We are therefore led to the conclusion that such an *internal layer* is parabolic in nature and that its width is $O(\sqrt{\epsilon})$. We again refer the reader to [1] for further justification.

In the next section we analyze the behavior of a standard central difference scheme when there is an internal layer tilted at an angle to the grid, and we show that the numerical approximation introduces downstream oscillations unless the internal layer is resolved. Therefore, we must use either a fine grid, an artificial increase of the viscosity ϵ, or a grid aligned with the layer. Here we are discussing a grid effect, in [13] Hedstrom and Osterheld showed that the numerical errors for a coarse grid aligned with an internal layer are minimal even at large cell Reynolds numbers.

In Section 3 we present an algorithm for the construction of an orthogonal grid with one coordinate direction aligned to the vector field (a,b). This mapping requires the solution of the telegraphers' equation. In Section 4 we introduce a domain decomposition for a problem (1.1) with an internal layer and an ordinary boundary layer. In this domain decomposition the ordinary boundary layer and the internal layer have their own subdomains, and there is a separate subdomain for the region where these layers interact. In addition, in each subdomain a separate numerical method is used, depending on the local asymptotic behavior of the solution.

2 A layer tilted to the grid.

In this section we use a heuristic argument based on the modified equation to show why it is generally unwise to permit an internal layer not to be aligned with the grid. Specifically, we show that the standard central-difference scheme has grid effects which are modelled by a modified equation in the style of Warming and Hyett [16]. See Griffiths and Sanz-Serna [10] for a more modern exposition on modified equations. We shall see that the solutions of the modified equation are integrals of Airy functions, multiplied by a decaying exponential. The oscillations of this Airy function may or may not be completely damped by the exponential, depending on the values of a dimensionless parameter. We also derive the modified equation

for the upwind difference scheme, and as may be expected, we find that upwinding adds numerical diffusion.

For the discussion here we restrict our attention to the special case when the coefficients a and b in (1.1) are constant and the source term F vanishes. Then for convection with velocity V in the direction $(\cos\theta, \sin\theta)$ we have the convection-diffusion equation

$$V\cos\theta\,\partial_x u + V\sin\theta\,\partial_y u = \epsilon\,\Delta u. \tag{2.1}$$

The reduced equation for (2.1) is

$$V\cos\theta\,\partial_x U + V\sin\theta\,\partial_y U = 0, \tag{2.2}$$

and its characteristic curves are given by

$$\frac{dx}{ds} = V\cos\theta, \qquad \frac{dy}{ds} = V\sin\theta. \tag{2.3}$$

For the discussion here it suffices to restrict our attention to directions $0 \le \theta \le \pi/4$. We remark that the special case $\theta = 0$ of flow parallel to the grid was examined by Hedstrom and Osterheld [13].

For (2.1) we use a rectangular domain

$$\Omega = \{(x,y): 0 < x < 1, 0 < y < 1\}. \tag{2.4}$$

Thus, under the conditions that $0 \le \theta \le \pi/4$ the inflow boundary is at $x = 0$ and at $y = 0$, and the other two sides of the rectangle comprise the outflow boundary. On the inflow boundary we select a point of discontinuity y_0, and we impose the conditions

$$u = \begin{cases} 0.5(1 + \operatorname{sgn}(y - y_0)) & \text{for } x = 0, \\ 0 & \text{for } y = 0. \end{cases} \tag{2.5}$$

The discontinuity in the boundary data at y_0 induces an internal layer along the characteristic curve $x\sin\theta - (y - y_0)\cos\theta = 0$. In fact, the solution U to the reduced equation (2.2) with boundary data (2.5) is given by

$$U = \frac{1}{2} - \frac{1}{2}\operatorname{sgn}(x\sin\theta - (y - y_0)\cos\theta). \tag{2.6}$$

In order to minimize ordinary boundary layers along the outflow boundary, we impose the reduced equation (2.2) as boundary condition at $x = 1$ and at $y = 1$.

Consider the standard central-difference scheme for (2.1). We impose a square grid on Ω with mesh size h, and we define the shift operators

$$T_x v(x,y) = v(x + h, y), \qquad T_y v(x,y) = v(x, y + h). \tag{2.7}$$

With this notation the central-difference approximation to (2.1) is

$$\frac{V\cos\theta}{2h}(T_x - T_x^{-1})v + \frac{V\sin\theta}{2h}(T_y - T_y^{-1})v = \epsilon\, Dv, \tag{2.8}$$

where D denotes the discrete Laplacian

$$D = \frac{1}{h^2}(T_x + T_y + T_x^{-1} + T_y^{-1} - 4I).$$

On the inflow boundary Γ_I the boundary conditions for (2.8) are (2.5). On the outflow boundary Γ_O we use an upwind discretization of (2.2).

The modified equation for (2.8) is best written in terms of the rotated coordinate system aligned with the flow direction

$$\begin{aligned} s &= x\cos\theta + (y - y_0)\sin\theta, \\ t &= -x\sin\theta + (y - y_0)\cos\theta. \end{aligned} \tag{2.9}$$

We also introduce scalings of s and t in order to derive a modified equation in dimensionless form and to identify the pertinent parameters. It happens that for (2.1) or (2.8) on the halfplane $x > 0$ there is no natural length scale in the direction of the flow (the s-direction). One may as well use a length scale $L = 1$. For the rectangular domain Ω defined in (2.4) it is reasonable to take L to be the width of Ω ($L = 1$) or the width of Ω in the s-direction ($L = \sec\theta$). We shall see that the natural scalings for the modified equation corresponding to the central difference method (2.8) are

$$\begin{aligned} s &= L\sigma, \\ t &= \tau\left(\frac{L\epsilon}{V}\right)^{1/2}. \end{aligned} \tag{2.10}$$

Furthermore, the important dimensionless parameters for (2.8) are the cell Reynolds number

$$R_h = \frac{hV}{\epsilon} \tag{2.11}$$

and the degree of streamwise resolution

$$\gamma = \frac{h}{L}. \tag{2.12}$$

In terms of these parameters the modified equation for (2.8) is given by the following theorem.

Theorem. *Suppose that* $0 \le \theta \le \pi/4$. *Suppose also that* $\gamma \ll 1$ *and that* $\gamma \ll R_h \ll 1/\gamma$. *Then the modified equation for* (2.8) *is*

$$\partial_\sigma v = \partial_\tau^2 v - \frac{\sin(4\theta)}{24}\gamma^{1/2}R_h^{3/2}\,\partial_\tau^3 v + \left(\frac{\gamma}{R_h} + \frac{\gamma R_h}{48}(3 + \cos(4\theta))\right)\partial_\sigma^2 v. \tag{2.13}$$

Remarks. The restriction that $\gamma = h/L \ll 1$ is reasonable for numerical computations, since we would want features in the streamwise direction to be resolved. The condition that $\gamma \ll R_h \ll 1/\gamma$ is also ordinarily satisfied in computations. We have written the modified equation in the form (2.13) in order to provide uniformity as $\sin(4\theta) \to 0$. The grid-induced oscillations appear only when $\sin(4\theta) \neq 0$ and when R_h is moderately large. (Remember that we require $R_h\gamma \ll 1$.) Under the condition that $R_h \sin(4\theta)$ is bounded away from zero, the modified equation (2.13) takes the simpler form

$$\partial_\sigma v = \partial_\tau^2 v - \frac{\sin(4\theta)}{24}\gamma^{1/2} R_h^{3/2}\, \partial_\tau^3 v. \tag{2.14}$$

In (2.14) the parameter

$$\beta = \frac{\sin(4\theta)}{24}\gamma^{1/2} R_h^{3/2} \tag{2.15}$$

measures the importance of the grid-induced numerical dispersion relative to the physical diffusion, and no numerically induced oscillations will be observed if β is sufficiently small. For boundary data $v = \mathrm{sgn}(\tau)$ at $\tau = 0$ the solution of (2.14) may be expressed in terms of the Airy function, as is shown by Chin and Hedstrom [3]. In fact, a Fourier transformation with respect to τ shows that

$$v(\sigma,\tau) = \frac{1}{2} + \int_{-\infty}^{\infty} \frac{1}{i2\pi\omega} \exp\left\{i\beta\sigma\omega^3 - \sigma\omega^2 + i\tau\omega\right\}\, d\omega. \tag{2.16}$$

The reference [3] also provides figures and tables of the integrals (2.16) for various values of β. The upshot is that whether or not there are oscillations depends on a parameter

$$\alpha = \frac{2\sigma^{1/3}}{(3\beta)^{2/3}}. \tag{2.17}$$

If $\alpha > 2$, the diffusion is dominant, and there are no oscillations. For $\alpha < 2$, however, there is a sequence of damped oscillations below the layer ($\tau < 0$). Because α is an increasing function of σ, as we proceed downwind σ increases and the diffusion eventually removes the oscillations.

Note with regard to the applicability of the modified equation that the internal layer is many grid cells wide and that the oscillations have wavelengths spanning many grid cells. This behavior makes the modified equation applicable, in that the derivation of a modified equation is based on the assumption that the numerical solution is smooth relative to the grid. The user of modified equations must always keep in mind that they are utterly useless in predicting variations in the numerical solution on the scale of 2 or 3 grid sizes or shorter.

Finally, we also remark that the upwind difference scheme

$$V\frac{\cos\theta}{h}(I - T_x^{-1})u + V\frac{\sin\theta}{h}(I - T_y^{-1})u = \epsilon\, Du$$

with the scalings (2.10) has the modified equation

$$\partial_\sigma v = \alpha_1\, \partial_\tau^2 v + \alpha_2\, \partial_\sigma^2 v$$

with

$$\begin{aligned}\alpha_1 &= 1 + \tfrac{R_h}{2\sqrt{2}} \sin(2\theta) \cos\left(\tfrac{\pi}{4} - \theta\right), \\ \alpha_2 &= \tfrac{\gamma}{R_h} + \tfrac{\gamma R_h}{48}(3 + \cos(4\theta) + 24(\cos^3\theta + \sin^3\theta)).\end{aligned}$$

The most significant numerical viscosity added by the grid effect is the deviation of α_1 from 1.

Proof of the theorem. The idea of the modified equation is to make an ansatz that the solution of the difference scheme is smooth enough to be represented by a small number of terms of its Taylor expansion and to use this expansion to identify a partial differential equation which approximates (2.8) more closely than the original equation (2.1) does.

Thus, we begin with the assumption that some smooth function v is a solution of (2.8). In this case the word 'smooth' is taken to mean that we may use Taylor approximations such as

$$T_x v = v + h\,\partial_x v + \frac{h^2}{2}\,\partial_x^2 v + \frac{h^3}{6}\,\partial_x^3 v + \frac{h^4}{24}\,\partial_x^4 v \tag{2.18}$$

for the terms in (2.8).

That is, we choose to neglect terms in the Taylor series approximation to (2.8) of order h^5 and higher. We therefore obtain the equation

$$\begin{aligned}V\cos\theta\left(\partial_x v + \tfrac{h^2}{6}\,\partial_x^3 v\right) + V\sin\theta\left(\partial_y v + \tfrac{h^2}{6}\,\partial_y^3 v\right) \\ = \epsilon\left(\partial_x^2 v + \partial_y^2 v + \tfrac{h^2}{12}(\partial_x^4 v + \partial_y^4 v)\right).\end{aligned}$$

The rotation of coordinates (2.9) then gives

$$V\partial_s v + \frac{Vh^2}{6} L_3[v] = \epsilon(\partial_s^2 v + \partial_t^2 v) + \frac{\epsilon h^2}{12} L_4[v] \tag{2.19}$$

with

$$\begin{aligned}L_3[v] &= \tfrac{1}{4}(3 + \cos(4\theta))\,\partial_s^3 v - \tfrac{3}{4}\sin(4\theta)\,\partial_s^2\partial_t v + \tfrac{3}{2}\sin^2(2\theta)\,\partial_s\partial_t^2 v + \tfrac{1}{4}\sin(4\theta)\,\partial_t^3 v, \\ L_4[v] &= \tfrac{1}{4}(3 + \cos(4\theta))(\partial_s^4 v + \partial_t^4 v) - \sin(4\theta)(\partial_s^3\partial_t v - \partial_s\partial_t^3 v) + 3\sin^2(2\theta)\partial_s^2\partial_t^2 v.\end{aligned}$$

Because we are interested in the effects of the internal layer, we expect derivatives of v in the t-direction (perpendicular to the layer) to be significantly larger than derivatives in the s-direction. The scalings (2.10) are selected to balance the terms $\partial_s v$ and $\partial_t^2 v$ in (2.19). Thus, upon substituting (2.10) into (2.19) and dropping terms smaller than $O(\gamma R_h)$, we obtain

$$\partial_\sigma v = \partial_\tau^2 v - \beta\, \partial_\tau^3 v + \frac{\gamma}{R_h}\partial_\sigma^2 v + \frac{\gamma R_h}{48}(3 + \cos(4\theta))\, \partial_\tau^4 v \tag{2.20}$$

with β as defined by (2.15).

The inexperienced user of modified equations may expect (2.20) to serve as a modified equation for (2.8). We cannot use it because the term involving $\partial_\tau^4 v$ renders (2.20) unstable to high-frequency perturbations. The use of such a modified equation would predict numerical instabilities where there are none, and it is an instance of a modified equation not conforming to the difference scheme for phenomena of short wave length. The term $\partial_\tau^4 v$ appears in (2.20) because we stopped the Taylor expansion (2.18) at $\partial_x^4 v$, and we went that far because the coefficient β of $\partial_\tau^3 v$ in (2.20) is zero when $\sin(4\theta) = 0$. That is, we must replace $\partial_\tau^4 v$ by something reasonable but harmless when β is near zero, and for other values of β it need only be something harmless. Because $\partial_\sigma v \approx \partial_\tau^2 v$ when $\beta \approx 0$, the substitution we make to render $\partial_\tau^4 v$ harmless is that $\partial_\tau^4 v \approx \partial_\sigma^2 v$. In this way a high-frequency instability is converted into an increase of dissipation in the streamwise direction, and it produces our modified equation (2.13). (This trick was also used in [13] in the special case $\theta = 0$.)

Remarks to mathematicians. The above argument contains some sleight of hand. In particular, the domain Ω was replaced by the halfspace $s > 0$ or, equivalently, $\sigma > 0$. This change removes any ordinary boundary layer which may be present at the outflow. In addition, boundary data for (2.13) are to be applied at the rotated boundary $s = 0$. We expect these distortions to introduce discrepancies only near the point of discontinuity $(x, y) = (0, y_0)$. In particular, it appears from our computations that there needs to be a slight shift of coordinates. See the comments concerning Fig. 1 below. We have also not shown that the solution of the modified equation (2.13) bears any resemblance to the solution of the difference scheme (2.8). Such a proof would probably proceed as in [13] with the replacement of Ω by the halfspace $x > 0$, followed by a Fourier transformation of (2.8) in the y-direction. The modified equation (2.13) shows that the canonical form of the integral representation of v is

$$v(\sigma, \tau) = \frac{1}{2} + \int_{-\infty}^{\infty} \frac{f(\omega)}{i2\pi\omega} \exp\left\{ia_3\omega^3 - a_2\omega^2 + ia_1\omega\right\} d\omega \tag{2.21}$$

with f and the a_j dependent on σ and τ. Furthermore, the integral (2.16) indicates that $f \approx 1$, $a_3 \approx \beta\sigma$, $a_2 \approx \sigma$, and $a_1 \approx \tau$ when $\sigma \gg 1$ and $|\tau| \ll 1$. The integral (2.16) derived from the modified equation (2.14) is merely a nonuniform asymptotic approximation which is valid when $|\tau| \ll 1$, $\sigma \gg 1$, and when β is bounded away from zero. We see from the form of (2.21) that a uniform asymptotic estimate would require investigation of the interaction of two saddle points and a pole. For the case when $\sin(4\theta) = 0$ the situation is simpler because

$a_3 = 0$ and there is only one saddle point and a pole. Uniform asymptotics for $\theta = 0$ are presented in Hedstrom and Osterheld [13].

A computational example. In our computations to illustrate these oscillations we located the point of discontinuity at $y_0 = 0.25$, we chose coefficients

$$V \cos\theta = 2, \qquad V \sin\theta = 1, \qquad \epsilon = 0.002,$$

and we used a mesh size of $h = 0.02$. This gives a cell Reynolds number of moderate size $R_h = 10\sqrt{5}$, and with $L = 1$ it gives $\gamma = 0.02$. The scaling (2.10) is therefore $\sqrt{L\epsilon/V} \approx 0.0946$, and the value of β in (2.15) is $\beta \approx 0.598$. The cross section at $x = 0.8$ is shown in Fig. 1, where the solution to (2.8) is shown as a solid curve and the Airy integral (2.16) is given as dashes. We must admit that in order to obtain such a good match of the curves, we had to shift the jump for the Airy integral from y_0 to $y_0 + h$. This could be because the Airy integral applies to the rotated coordinate system (s, t) given by (2.9). It should also be noted that there is a phase difference between the two curves in the oscillatory region. This is a well-known deficiency of modified equations, and it results from the nonuniformity of the asymptotic approximation. At the point $(x, y) = (0.8, 0.6)$ near the overshoot the value of the parameter α given by (2.17) is $\alpha \approx 1.294$. We have oscillations because $\alpha < 2$.

The numerical method we used to solve (2.8) is a combination of ideas from Elman and Golub [9] and from Chin and Manteuffel [6]. As in Elman and Golub, we introduce a red-black ordering on the grid points and do a cyclic reduction to obtain a nine-point scheme on the black grid points. This reduction produces a matrix much better conditioned for iterative methods. The iterative method used by Elman and Golub is point Jacobi, mostly because they impose no constraints on the direction of flow. In our example the flow is one-directional, so we follow Chin and Manteuffel in using line Gauss-Seidel with lines transversal to the flow, starting at the inflow boundary and marching downstream. We find that this scheme converges very rapidly, with the greatest speeds at high cell Reynolds numbers. (Perhaps, we should reiterate that the point of this section is to show that rapid solution of the matrix equation should not be the primary objective—its solution is a poor approximation to the solution of the differential equation when the parameter β in (2.15) is large.)

Let us remark that we have also solved (2.8) in a version with a discrete approximation to Neumann outflow boundary conditions

$$\begin{aligned} \partial_x u &= 0 \quad \text{for } x = 1, \\ \partial_y u &= 0 \quad \text{for } y = 1. \end{aligned} \tag{2.22}$$

We found this boundary condition to be satisfactory only for small cell Reynolds number, $R_h < 5$. Otherwise, there are additional small oscillations with period $2h$ induced by the mismatch at the outflow boundary $x = 1$.

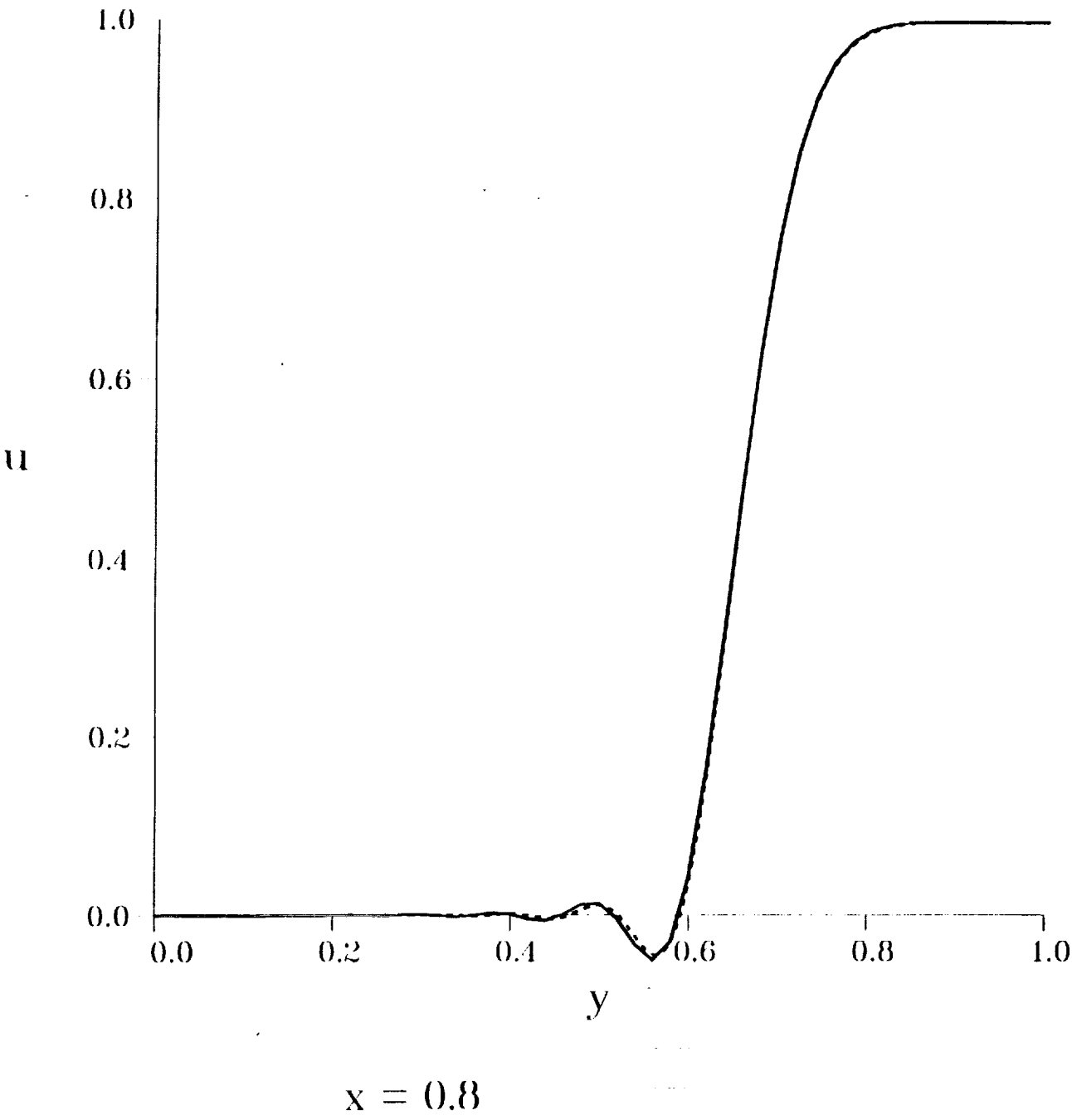

Fig. 1. Airy oscillations.

3 Curvilinear coordinates.

In this section we permit the coefficients a and b in (1.1) to depend on the position (x, y), and we present a numerical algorithm for generating an orthogonal coordinate system (a chart) aligned with the given vector field (a, b). Our coordinate system is derived from the characteristic curves. We remark that a somewhat different coordinate transformation based on characteristics was given by Chin *et al.* [5].

We again assume that the vector field (a, b) has no stagnation point, so that $|a| + |b|$ is bounded away from zero for all (x, y) in Ω. For purposes of constructing the mapping, it is convenient to do an initial scaling so that $a^2 + b^2 = 1$. One of our goals is to set up a mapping $(s, t) \mapsto (x, y)$ such that s follows the flow in the sense that there exists a positive function ϕ for which

$$\partial_s = \phi(a\,\partial_x + b\,\partial_y). \tag{3.1}$$

Because the vector $(-b, a)$ is orthogonal to (a, b), the orthogonality requirement (our second goal) amounts to the condition

$$\partial_t = \psi(-b\,\partial_x + a\,\partial_y) \tag{3.2}$$

for some positive function ψ. In a moment we show that the scale factors ϕ and ψ are not arbitrary.

In part, the construction of such a mapping is easy, because it is easy to integrate (3.1). All that is needed is to pick a convenient starting point (x_0, y_0) and to integrate the system

$$\begin{aligned} \frac{dx}{ds} &= a\phi, \qquad x = x_0 \text{ at } s = 0, \\ \frac{dy}{ds} &= b\phi, \qquad y = y_0 \text{ at } s = 0. \end{aligned} \tag{3.3}$$

This gives a curvilinear coordinate line in Ω corresponding to a constant value of t. The image of a line $s =$ constant may be obtained similarly by integrating

$$\begin{aligned} \frac{dx}{dt} &= -b\psi, \qquad x = x_0 \text{ at } t = 0, \\ \frac{dy}{dt} &= a\psi, \qquad y = y_0 \text{ at } t = 0. \end{aligned} \tag{3.4}$$

We still must ensure global consistency as follows. Let us traverse the edges of the curvilinear rectangle $s_0 < s < s_1$, $t_0 < t < t_1$, and we assume that this rectangle is contained in Ω. Denote the image of (s_0, t_0) as the vertex A. Suppose further that we integrate (3.3) from s_0 to s_1, arriving at the vertex C. We then integrate (3.4) from t_0 to t_1 and arrive at the vertex B opposite A. Let us now reverse the order by first integrating (3.4) from t_0 to t_1 to arrive at the vertex D and then integrate (3.3) from s_0 to s_1. Can we be certain that we again arrive at the vertex B? It happens that this global consistency question has

been answered [15], and that what is required is the vanishing of the Lie bracket $[\partial_s, \partial_t] = \partial_s\partial_t - \partial_t\partial_s$.

It is easy to see by a short computation that the vanishing of the Lie bracket $[\partial_s, \partial_t]$ is equivalent to the system of partial differential equations

$$\begin{aligned} \partial_s(a\psi) &= \partial_t(b\phi), \\ \partial_s(b\psi) &= -\partial_t(a\phi). \end{aligned} \tag{3.5}$$

Upon differentiating the products in (3.5) and solving for $\partial_s\psi$ and $\partial_t\phi$, we find that a necessary and sufficient condition for consistency is that

$$\begin{aligned} (a^2+b^2)\,\partial_s\psi &= \phi(a\,\partial_t b - b\,\partial_t a) - \psi(a\,\partial_s a + b\,\partial_s b), \\ (a^2+b^2)\,\partial_t\phi &= -\phi(a\,\partial_t a + b\,\partial_t b) + \psi(b\,\partial_s a - a\,\partial_s b). \end{aligned} \tag{3.6}$$

Note that if (a, b) has been scaled so that $a^2 + b^2 = 1$, then (3.6) takes the simpler form

$$\begin{aligned} \partial_s\psi &= \phi(a\,\partial_t b - b\,\partial_t a), \\ \partial_t\phi &= \psi(b\,\partial_s a - a\,\partial_s b). \end{aligned} \tag{3.7}$$

We recognize the system (3.7) as the telegraphers' equation, written in terms of Lie derivatives along the characteristic curves. Therefore, all that is needed for its solution is to prescribe values $\phi = 1$ at $t = 0$ and $\psi = 1$ at $s = 0$ and to march in the s and t-directions concurrently.

It should be emphasized that theoretical questions remain for this grid-generation scheme. In particular, there is no guarantee that the solutions ϕ and ψ will be positive at all points in Ω. This is important in that the Jacobian of the transformation (3.3–4) is given by $J = (a^2+b^2)\phi\psi$. We required at the outset that a^2+b^2 be bounded away from zero. Thus, if we are to maintain a nonzero Jacobian, we must take special measures whenever it happens that $\phi \leq 0$ or $\psi \leq 0$. One possibility is to back up and put a boundary on this local chart. We could then initialize a new chart and continue.

4 Domain decomposition for an internal layer.

In this section we present a computational example which uses domain decomposition to resolve an internal layer. At this point we have not yet implemented the algorithm described here, but the final report will have computations. In our algorithm we first identify the internal and boundary layers, and we then set up a domain decomposition to segregate them. The domain decomposition is carried out with overlapping grids using the tools of Chesshire and Henshaw [2]. We have added the modification that in some subdomains we use the grid-generation algorithm of Section 3.

As our domain Ω we use the square $0 < x < 1$, $0 < y < 1$, and on Ω we consider the convection-diffusion equation

$$(1+x)\,\partial_x u + (1-y)\,\partial_y u = \epsilon \Delta u. \tag{4.1}$$

As boundary conditions for (4.1) we prescribe $u = 0$ on the bottom of Ω ($y = 0$), $u = 1$ on the left-hand edge ($x = 0$), $u = 1$ on the top ($y = 1$), and $u = -1$ on the right-hand edge ($x = 1$).

Note that in (4.1) we have chosen coefficients so that there is no turning point in Ω. That is, we have $|1+x| + |1-y|$ bounded away from zero in Ω. Note also that by the discussion in Section 1 the inflow boundary Γ_I consists of the bottom $y = 0$ and the left-hand side $x = 0$ of the square Ω. Furthermore, the top of the square $y = 1$ is a tangential boundary Γ_T, and the right-hand edge $x = 1$ is an outflow Γ_O. The reduced equation is

$$(1+x)\,\partial_x U + (1-y)\,\partial_y U = 0, \tag{4.2}$$

and its boundary conditions are imposed on the inflow boundary Γ_I. It so happens that we can write down a formula for the solution U of (4.2), although this is not necessary for our domain-decomposition algorithm. The characteristic curves for (4.2) are the hyperbolas $(x-1)(y+1) = \text{const}$. Thus, the solution of the reduced equation (4.2) is

$$U = \begin{cases} 1 & \text{if } y > x/(x+1), \\ 0 & \text{if } y < x/(x+1). \end{cases}$$

This gives us an internal layer along the hyperbola $y = x/(x+1)$ and exponential boundary layers at the outflow boundary $x = 1$. It happens that we imposed boundary data along the tangential boundary Γ_T such that no boundary layer resides there. If there had been a boundary layer along Γ_T, we could have modified the domain decomposition described below so as to include its effects.

As the problem is stated, we need the following subdomains: (1) a square $\mathcal{B}$ of diameter $O(\epsilon)$ at the origin to cover the birth of the internal layer, (2) an internal-layer region

$$\mathcal{I} = \{(x,y): |y - x/(x+1)| < C\sqrt{\epsilon x}\}$$

with $O(\epsilon) < x < 1 - O(\epsilon)$, (3) three outflow boundary layers $\mathcal{O}$, one above the internal layer, one below it, and one interacting with it, (4) an outer region $\mathcal{H}$ above the internal layer on which $u \approx 1$, and (5) an outer region $\mathcal{H}$ below the internal layer on which $u \approx 0$.

In the two outer regions $\mathcal{H}$ we use a coordinate system derived from the characteristics, as described in Section 3. In the internal layer $\mathcal{I}$ we use a parabolic coordinate system imposed on the characteristics. (More precise details will be given in the final report.) Finally, in the birth $\mathcal{B}$ and boundary-layer regions $\mathcal{O}$ we use the methods given in the papers by Hedstrom and Howes [11] and [12]. The iterations are performed in the order: (1) the outer regions $\mathcal{H}$, (2) the birth region $\mathcal{B}$, (3) the internal layer $\mathcal{I}$, (4) the outflow boundary layers $\mathcal{O}$. The iterative schemes in the subdomains are as in [11] and [12].

4.1 Acknowledgments.

The work of the first author (D. L. B.) was supported by Los Alamos National Laboratory through the U. S. Department of Energy under contract W-7405-ENG 36. The work of the second and third authors (R. C. Y. C. and G. W. H.) was supported by the Applied Mathematical Sciences subprogram of the Office of Energy Research, U. S. Department of Energy by the Lawrence Livermore National Laboratory under contract number W-7405-ENG 48. The work of the fourth author (T. A. M.) was supported in part by NSF Grant DMS 8704169 and DOE Grant DE-FG02-90ER25086.

References

[1] K. W. Chang and F. A. Howes, *Nonlinear Singular Perturbation Phenomena: Theory and Applications*, Springer-Verlag, New York, 1984.

[2] G. Chesshire and W. D. Henshaw, 'Composite overlapping meshes for the solution of partial differential equations', *J. Comput. Phys.* **90** (1990), 1–64.

[3] R. C. Y. Chin and G. W. Hedstrom, 'A dispersion analysis for difference schemes: Tables of generalized Airy functions', *Math. Comput.* **32** (1978), 1163–1170.

[4] R. C. Y. Chin and G. W. Hedstrom, 'Domain decomposition: An instrument of asymptotic-numerical methods', to appear in the Proceedings of the Workshop on Asymptotics and Numerics, H. Kaper, ed., Marcel Dekker.

[5] R. C. Y. Chin, G. W. Hedstrom, F. A. Howes, and J. R. McGraw, 'Parallel computation of multiple-scale problem', pp. 136–153 in *New Computing Environments: Parallel, Vector and Systolic*, A. Wouk, ed., Society for Industrial and Applied Mathematics, Philadelphia, 1986.

[6] R. C. Y. Chin and T. A. Manteuffel, 'An analysis of block successive overrelaxation for a class of matrices with complex spectra', SIAM J. Numer. Anal. **25** (1988), 564–585.

[7] P. Colella and P. R. Woodward, 'The piecewise-parabolic method for gas dynamic simulations', *J. Comput. Phys.* **54** (1984), 174–201.

[8] W. Eckhaus, *Asymptotic Analysis of Singular Perturbations*, North-Holland, Amsterdam, 1979.

[9] H. C. Elman and G. H. Golub, 'Iterative methods for cyclically reduced non-self-adjoint linear systems', *Math. Comp.* **54** (1990), 671–700.

[10] D. F. Griffiths and J. M. Sanz-Serna, 'On the scope of the method of modified equations', *SIAM J. Sci. Stat. Comput.* **7** (1986), 994–1008.

[11] G. W. Hedstrom and F. A. Howes, 'A domain decomposition method for a convection diffusion equation with turning point', pp. 38–46 in *Domain Decomposition Methods,* T. F. Chan, R. Glowinski, J. Periaux, and O. B. Widlund, eds., Society for Industrial and Applied Mathematics, Philadelphia, 1989.

[12] G. W. Hedstrom and F. A. Howes, 'Domain decomposition for a boundary-value problem with a shock layer', pp. 130–140 in *Domain Decomposition Methods for Partial Differential Equations,* T. F. Chan, R. Glowinski, J. Periaux, and O. B. Widlund, eds., Society for Industrial and Applied Mathematics, Philadelphia, 1990.

[13] G. W. Hedstrom and A. Osterheld, 'The effect of cell Reynolds number on the computation of a boundary layer', *J. Comput. Phys.*, **37** (1980), 399–421.

[14] P. L. Roe, 'Discrete models for the numerical analysis of time dependent multidimensional gas dynamics', *J. Comput. Phys* **63** (1986), 458–476.

[15] M. Spivak, *Differential Geometry,* vol. 1, second ed., Publish or Perish, Houston, 1979.

[16] R. F. Warming and B. J. Hyett, 'The modified equation approach to the stability and accuracy of finite-difference methods', *J. Comput. Phys.* **14** (1974), 159–179.

Interface Conditions for Domain Decomposition With Radical Grid Refinement

Jeffrey S. Scroggs[1]
Department of Mathematics
North Carolina State University
Raleigh, NC

Abstract

Interface conditions for coupling the domains in a physically motivated domain decomposition method are discussed. The domain decomposition is based on an asymptotic-induced method for the numerical solution of hyperbolic conservation laws with small viscosity. The method consists of multiple stages. The first stage is to obtain a first approximation using a first-order method, such as the Godunov scheme. Subsequent stages of the method involve solving internal-layer problems via a domain decomposition. The method is derived and justified via singular perturbation techniques.

1 Introduction

This is a report on a preliminary investigation of conditions for the interfaces between subdomains when solving partial differential equations. The analysis for the method is a combination of asymptotics and numerical analysis. The result is a physically motivated domain decomposition method where different partial differential equations may be solved in different domains. Since different modeling equations are in different subdomains for the same problem, we call this *heterogeneous* domain decomposition. The numerical treatment of interface conditions between the subdomains must be addressed. The approach here is to examine the physics reflected in the numerical method used within the subdomains and guarantee that this same physics is reflected in the interface treatment.

The method is best suited to partial differential equations that contain regions of singular behavior. A typical situation is when there are narrow regions where the variation in the solution is large. Such regions are called *boundary layers* or *transition layers* depending on whether they are near a boundary or inside the interior of the domain. Examples of such situations are laminar flow of a slightly viscous fluid or combustion with high activation energy. Classical schemes applied to these types of situations generally fail to correctly describe the behavior inside the layers. This difficulty is overcome by utilizing asymptotic analysis that reflects the physics of the problem. Here we present and motivate the domain decomposition method, but the details of the analysis are presented elsewhere [7].

There have been some intersting results regarding interface conditions for heterogeneous domain decomposition where Euler equations are coupled with Navier-Stokes equations [9],

[1]Research conducted at ICASE, NASA Langley Research Center, Hampton, Virginia, supported by NASA Contract No. NAS1-18605.

and where viscous and inviscid equations where coupled [2, 4]. Many of the basic ideas relating to asymptotic analysis and numerical methods that utilize domain decomposition are found in [10]. These ideas were incorporated into a parallel numerical method in [5]. Specific application to conservation laws have been developed in [1]. There are other important works in these areas–these references are only a small sample of the literature.

The coupling of the problems in the subdomains is based on a balance of the flux across the interface. Each subdomain is treated as a control volume, and the flux into and out-of the control volume is balanced. This is similar to the flux-differencing methods used within the subdomains. The result is a numerical method with no visual artifacts. This numerical treatment of the interface is an extension (to heterogeneous domain decomposition) of the work by Osher and Saunders [11]. We expect extension of this method for the interfaces to work for two dimensional heterogeneous domain decomposition, since it was used for a two-dimensional homogeneous domain decomposition method that utilizes adaptive refinement [8].

2 Problem Setting and Domain Decomposition Motivation

Consider the Cauchy problem

$$\begin{cases} \frac{\partial U}{\partial t} + \frac{\partial}{\partial x} F(U) = \epsilon \frac{\partial}{\partial x} \left(P(U) . \frac{\partial U}{\partial x} \right) & \text{for} \quad (x,t) \in \Omega \\ \\ U(x,0) = V(x) & \text{for} \quad x \in \mathbb{R}. \end{cases} \tag{2.1}$$

Here the solution $U \in \mathbb{R}^n$ is a vector-valued function with n components, the domain is $\Omega = \mathbb{R} \times]0, T[$ and $\epsilon << 1$ is a small parameter.

We assume that V is piecewise smooth. We also assume F and P are regular functions of U. We suppose that P is a *suitable viscosity matrix* [3] for the shocks of the associated inviscid problem

$$\begin{cases} \frac{\partial U^0}{\partial t} + \frac{\partial}{\partial x} F(U^0) = 0 & \text{for} \quad (x,t) \in \Omega \\ \\ U^0(x,0) = V(x) & \text{for} \quad x \in \mathbb{R}. \end{cases} \tag{2.2}$$

Namely, a shock-wave solution to (2.2) can be obtained as a limit of progressive wave solutions of (2.1). Problem (2.1) is a parabolic-hyperbolic singular perturbation problem driven by (2.2).

The regions where the solutions to the associated inviscid problem fail to be good approximations to the solution of the full problem are the regions where we use a subdomain to localize the behavior of the solution. Thus, we have two types of domains. The first type of domain is located where the regular expansion

$$U_{\text{as}}^{\text{outer}} = U^0 + \epsilon U^1 + \epsilon^2 U^2 + \dots \tag{2.3}$$

for U is valid and the solution is smooth. The second type of domain is where the solution exhibits singular behavior and the regular expansion for U is no longer valid.

We substitute $U_{\text{as}}^{\text{outer}}$ in the differential equation of (2.1) and use identification in ϵ to obtain that U^0 must be a solution of (2.2). The inviscid problem (2.2) has many weak solutions; it is possible to uniquely define U^0 by considering the problem that governs U^1 [7].

The failure of the regular expansion is reflected by some of the terms in the PDE governing U^0 being significantly larger than other terms. Typically, the term $RHS(U^0)$ will become unbounded as the small parameter ϵ tends to zero. For finite ϵ, a large $RHS(U^0)$ would indicate that the region should be covered by a subdomain in which we apply techniques designed to capture the singular behavior of the solution. We describe how to use a measure of the numerical approximation of $RHS(U^0)$ to place the subdomain boundaries in a later section of this manuscript.

2.1 Problem in the Singular Region

So that we can handle the regions where solutions to problem (2.1) contain shocks that interact with other singularities we use a brute force approach that will capture all possible behavior of the solution. The approach is to use the coordinate system

$$\xi = \frac{x}{\epsilon}, \quad \tau = \frac{t}{\epsilon}$$

in the regions with shocks. We will present and motivate the domain decomposition method, but the details of the analysis are presented elsewhere [7, 6]. Under this transformation the PDE that governs the solution becomes

$$\frac{\partial \tilde{U}}{\partial \tau} + \frac{\partial}{\partial \xi} F(\tilde{U}) = \frac{\partial}{\partial \xi} \left(P(\tilde{U}) \cdot \frac{\partial \tilde{U}}{\partial \xi} \right), \tag{2.4}$$

where $\tilde{U}(\xi, \tau) = U(x, t)$. This is the equation that is solved in the singular region.

This scaling is most appropriate for regions where shock-layers are interacting with other non-smooth physical phenomena. Because the transformation *a priori* resolves all of the physics. This is reflected by all of the terms in (2.4) having magnitude of order unity or smaller. In general, this method is overkill, similar to using a shotgun to dispatch a housefly. We choose to study only this brute-force approach so that we concentrate on one type of interface. Other treatments that include more of the physics are possible [7]. They can result in more efficient numerical methods than the one discussed here.

The boundary condition at the interface is to impose that the viscous equation from problem (2.1) be the model at the interface between the subdomains. The computational implications of this condition is discussed in §4.

3 Conservative Discretizations

It is important for the discretization techniques to satisfy a discrete conservation relation. One can verify that if the discretizations can be written in the form

$$z_i^{k+1} = z_i^k - \lambda(h_{i+1/2} - h_{i-1/2}),$$

then the method satisfies the appropriate conservation relations. Here we use flux differencing methods based on a finite-volume formulation of the problem.

We will discuss the differencing method for the outer region subdomain where the solution is smooth first. Let W_0 be the discrete numerical approximation to U^0. We use a first-order finite-volume method. This method assumes that the value $W_{0,i}^k$ is an approximation to the average of the desired function U^0 over the spatial interval $]x_{i-1/2}, x_{i+1/2}]$ at time $t = k\Delta t$. The method can also be categorized as a *flux differencing* technique since the general form of the discrete analogue to the original PDE can be written

$$W_{0,i}^{k+1} = W_{0,i}^k - \lambda(F_{i+1/2}^k - F_{i-1/2}^k) \tag{3.5}$$

where

$$F_{i+1/2}^k \approx F(W_{0,i+1/2}^k).$$

Here the fluxes are based on the first-order Godunov scheme; thus, the flux f_j for component w_j of W_0 is approximated as

$$f_{j,i+1/2}^k = \frac{1}{2}\left[f_j(W_{0,i}^k) + f_j(W_{0,i+1}^k) - \alpha_i(W_{j,i+1} - W_{j,i})\right] \tag{3.6}$$

where α_i is an approximation of the upper bound on the local speed of sound.

The discretization that is used for the numerical method in the shock-layer region is a modification of the treatment used for the outer region. We have used a coordinate transformation that creates a smooth problem for this subdomain. Let $\tilde{W}_0$ be the first order numerical approximation to $\tilde{U}$. Let $\tilde{W}_{0,i}^{\tilde{k}}$ be an approximation to the the average of the desired function $\tilde{U}$ over the spatial interval $]\xi_{i-1/2}, \xi_{i+1/2}]$ at time $\tau = \tilde{k}\Delta\tau$. The flux differencing technique is

$$\tilde{W}_i^{\tilde{k}+1} = \tilde{W}_i^{\tilde{k}} - \tilde{\lambda}(\tilde{F}_{i+1/2}^{\tilde{k}} - \tilde{F}_{i-1/2}^{\tilde{k}}) \tag{3.7}$$

where

$$\tilde{F}_{i+1/2}^{\tilde{k}} \approx F(\tilde{W}_{i+1/2}^{\tilde{k}}) \quad \frac{\partial \tilde{W}_{i+1/2}^{\tilde{k}}}{\partial \xi}$$

The particular discrete form for each component of the flux is obtained using a formula similar to that of Equation (3.6).

We are not restricted to this particular numerical discretization; however, the numerical treatment of the interface will possibly need to be modified for different numerical treatments of the problems within the subdomains.

One can verify that the flux differencing methods given above satisfy the discrete conservation relation. What remains is to formulate the conditions at the interface so that the relation will be satisfied globally.

4 Treatment of the Interface

Using the shock-layer coordinates with $\Delta\xi = C\Delta x$ will result in C/ϵ points in the shock-layer for each point in the outer region. Here, a typical value for ϵ is .01; hence, this results in a *radical* grid refinement for the shock-layer. For the numerical method, since there will be many grid points in the shock-layer for each point in the outer-region, we will refer to the shock-layer grid as the refined grid, and the outer region grid will be called the coarse grid. The temporal coordinate will also be stretched, resulting in the situation outlined in Fig. 4.1.

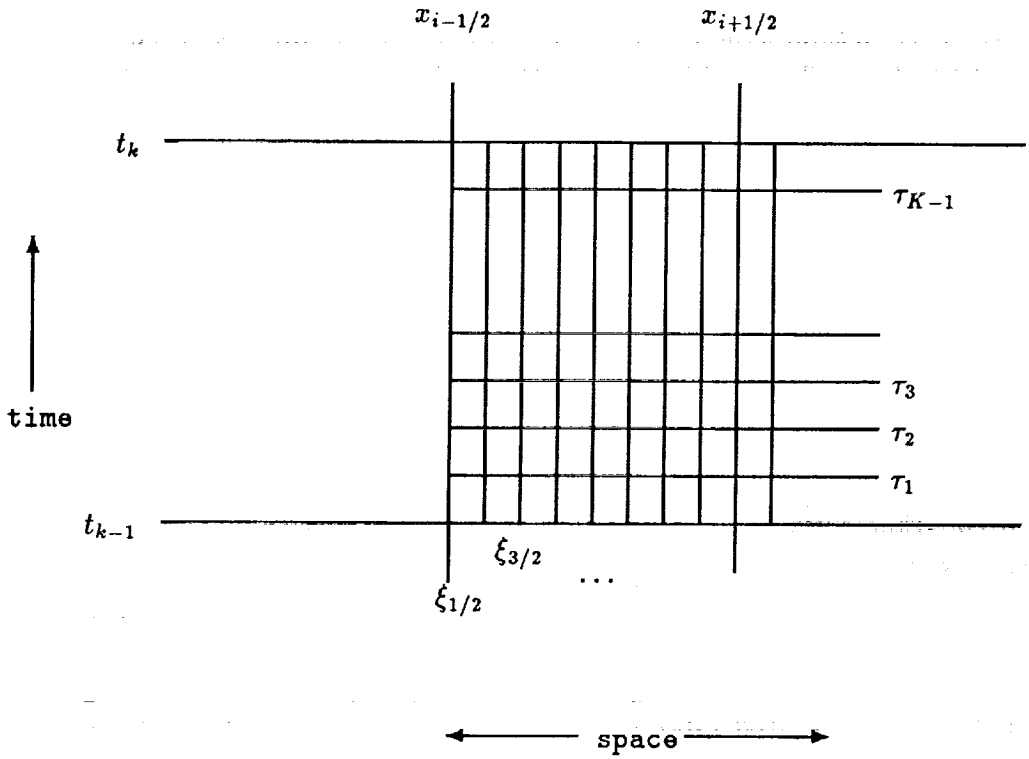

Figure 4.1: Interface at the left boundary

4.1 Flux Treatment of Interface

As in [11], we view the interface treatment as a predictor-corrector method on the coarse mesh. We start at time $t = t^k$. The coarse-grid values are defined everywhere, and are the average of the corresponding fine-grid values when the coarse-grid volume element is within the fine-grid region.

The steps for the first order method are outlined in Algorithm 1 below. At time step k, the shock-layer has $\bar{N}(k)$ points in the interior of the region and a ghost point on each

For $k = 1, \ldots$.

I. March W_0 from t_{k-1} to t_k based on scheme (3.5).

II. Detection.

A. Compute the residual on the coarse mesh.

B. Mark regions that should be refined. (Let this be the region between $x_{i_L-1/2}$ and $x_{i_R+1/2}$.

A. Modify shape of refined region.

III. March the shock-layer region from t_k to t_{k+1}. For $\tilde{k} = 1$ to K

1. Form the initial condition in newly refined regions.
2. Use linear interpolation to compute the ghost values of $\tilde{W}_O^{\tilde{k}}$
3. March $\tilde{W}_0$ to $\tau_{\tilde{k}+1}$ based on scheme (3.7).

IV. Project $\tilde{W}_0$ onto W_0.

V. Correct values $W_{0,L}^k$ and $W_{0,R}^k$ based on the shock-layer fluxes.

ALGORITHM 1 *Numerical Method.*

side of the refined region. There are a few points that need to be clarified in this algorithm. The interpolation to obtain ghost values (i.e. $\tilde{W}_{0,\tilde{0}}^{\tilde{k}}$) is bi-linear interpolation based on $\tilde{W}_{0,\tilde{1}}^{\tilde{k}-1}$, $W_{0,L-1}^{k-1}$ and $W_{0,L-1}^k$. The initial condition for this problem is derived by imposing mass conservation; thus, the fine-grid values are all initialized to the value of the solution at the cell center. Improvements in the initialization procedure is a subject of further research.

The correction of the coarse-grid values in Step VI is to use the same discretization that was used when the values were originally computed, but to modify the fluxes at the boundary of the domain to reflect what happened on the refined region. That is, to update $W_{0,L}^k$, we would use scheme (3.5) with (3.6) for $F_{L-1/2}^{k-1}$, but we would compute $F_{L+1/2}^{k-1}$ with the formula

$$F_{L+1/2}^{k-1} = \frac{1}{K} \sum_{\tilde{k}=0}^{K-1} \tilde{F}_{\tilde{0}}^{\tilde{k}}.$$

One may verify that this results in a globally conservative method. Also, this treatment of the boundary is consistent with the boundary conditions imposed in §2.1. Namely, this treatment of the interface is consistent with the viscous equation from problem (2.1) being the model at the interface between the subdomains.

4.2 Dirichlet Treatment of Interface

As a comparison to the flux boundary condition, we also implemented the heterogeneous domain decomposition method with dirichlet boundary conditions at the interface. This

is an interesting comparison, since there was little difference in the results when the two different treatments of the interface were used (this is discussed in §6).

5 Detection of Interface

We present the detection of the interface for the sake of completeness. Detection of the interface based on computational data results in a method that can have a different location of the internal-layer subdomain for each time step. The detection for the numerical method is based on obtaining an approximation to

$$\frac{\partial W_0}{\partial t} + \frac{\partial F(W_0)}{\partial x} - \epsilon \frac{\partial}{\partial x}\left(P(W_0)\frac{\partial W_0}{\partial x}\right).$$

This term is the residual from using W_0 as an approximation to the solution of (2.1). The residual is of magnitude $O(\Delta x^{-1})$ in either a shock layer or in a zone where a shock interacts with other singularities.

It is also possible to use an approximation of the viscous term $\frac{\partial^2}{\partial x^2} W_0(\cdot, t_K)$ to localize some of the singularities. For example, this viscous term will be of order $O(\Delta x^{-1})$ in a shock layer or in a zone of interaction. This method is not as reliable as using the residual, however. Other types of behavior can be located and identified using these techniques [7].

6 Application to the Isentropic Gasdynamic Equations

In this section we examine the interface treatments on the viscous isentropic gasdynamic equations

$$\frac{\partial u}{\partial t} - \frac{\partial v}{\partial x} = 0$$

$$\frac{\partial v}{\partial t} - \frac{\partial}{\partial x}\left(\frac{1}{u^\gamma}\right) = \epsilon \frac{\partial}{\partial x}\left(\frac{\partial u}{\partial x}\right).$$

Here u is the inverse of the density and v is the velocity. These equations are obtained from the conservation of mass and momentum in Lagrangian coordinates assuming that u is equal to the pressure raised to the $-1/\gamma$th power (the perfect gas law). The experiments were run with $\gamma = 2.2$.

The problem is a right-traveling shock interacting with and a left-traveling rarefaction, both of which eminate from the origin. An analytic self-similar solution (a rarefaction eminating from the origin) to the inviscid isentropic gasdynamic equations is given by

$$u(x,t) = \gamma^{1/(\gamma+1)}\left(\frac{x}{t}\right)^{-2/(\gamma+1)} \tag{6.8}$$

$$v(x,t) = \frac{-2\gamma^{1/(\gamma+1)}}{\gamma-1}\left(\frac{x}{t}\right)^{\frac{\gamma-1}{\gamma+1}} + const. \tag{6.9}$$

An initial condition with a shock and rarefaction eminating from the origin is constructed by connecting left values to middle values with a rarefaction. The middle values are connected to the right values with a shock. Thus, the initial condition is given by

$$u(x,0) = \begin{cases} U_L, & \text{for } x < 0 \\ U_R, & \text{for } x \geq 0 \end{cases} \tag{6.10}$$

$$v(x,0) = \begin{cases} V_L, & \text{for } x < 0 \\ V_R, & \text{for } x \geq 0 \end{cases} \tag{6.11}$$

where

$$U_L = 1.4709, \qquad U_R = 2.5000, \qquad V_L = 1.0388, \qquad V_R = 0.8050.$$

The middle value of the solution between the shock and rarefaction is $(U_M, V_M) = (1.973, 1.356)$. We remark that the middle values were was chosen using the Rankine-Hugoniot condition

$$\frac{V_M - V_R}{U_R - U_M} = \frac{1/U_R^\gamma - 1/U_M^\gamma}{V_R - V_M}.$$

We expect the the viscous perturbation to have little or no effect on the speed at which shocks and rarefactions travel; thus, we will compare the viscous solutions to the solutions given above.

The method was run with $\epsilon = .01$. The discretization parameters for numerical solution in the outer region have CFL number $\Delta t/\Delta x = .1$, and $\Delta x = .02$. The discretization on the scaled coordinates inside the shock-layer is based on $\Delta\xi = .1$, with the CFL condition $\Delta\tau/\Delta\xi \leq .025$ and the stability condition $\Delta\tau/\Delta\xi^2 \leq .1$. These values are well within the limits imposed for the stability of the finite difference methods.

Figure 6.2 depicts the evolution of the internal-layer subdomain when the two different boundary conditions are used. The errors generated by using the dirichlet boundary condition when the rarefaction is trying to exit the internal-layer subdomain result in a larger computed second derivative, and the detection scheme kept the rarefaction inside the internal-layer much longer. The solution projected onto the coarse grid at the end of the computations showed little difference between the two methods (Fig. 6.3). The primary difference is the visual artificats at the boundary of the internal-layer subdomain at the point when the rarefaction is exiting the subdomain (Fig. 6.4).

7 Conclusion

Clearly the best interface condition is the flux-based treatment; however, the dirichlet boundary conditions did not induce as many errors as expected. One explaination of the lack of errors may be that the internal-layer subdomain boundary moves fast enough that waves propagating out of the internal-layer subdomain are allowed to pass across the boundary by the oscillations in the boundary. More studies are planned with the goal to identify the precise nature of the errors associated with the interface treatments.

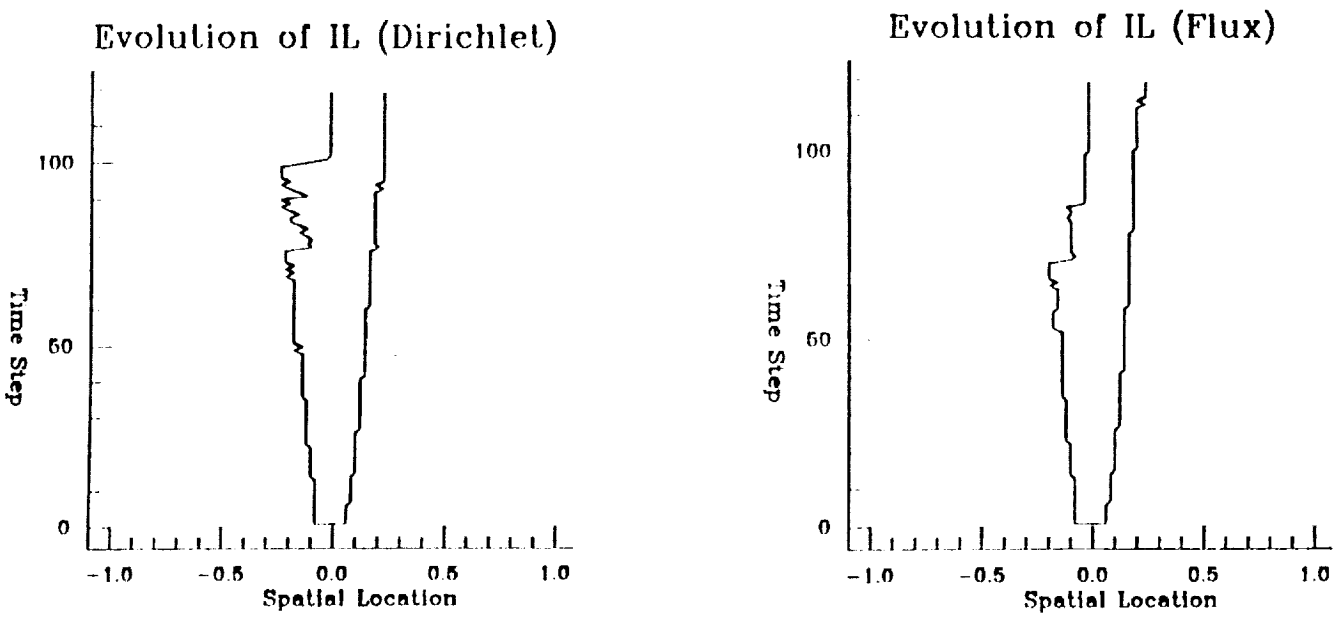

Figure 6.2: Evolution of the Internal-layer Subdomain.

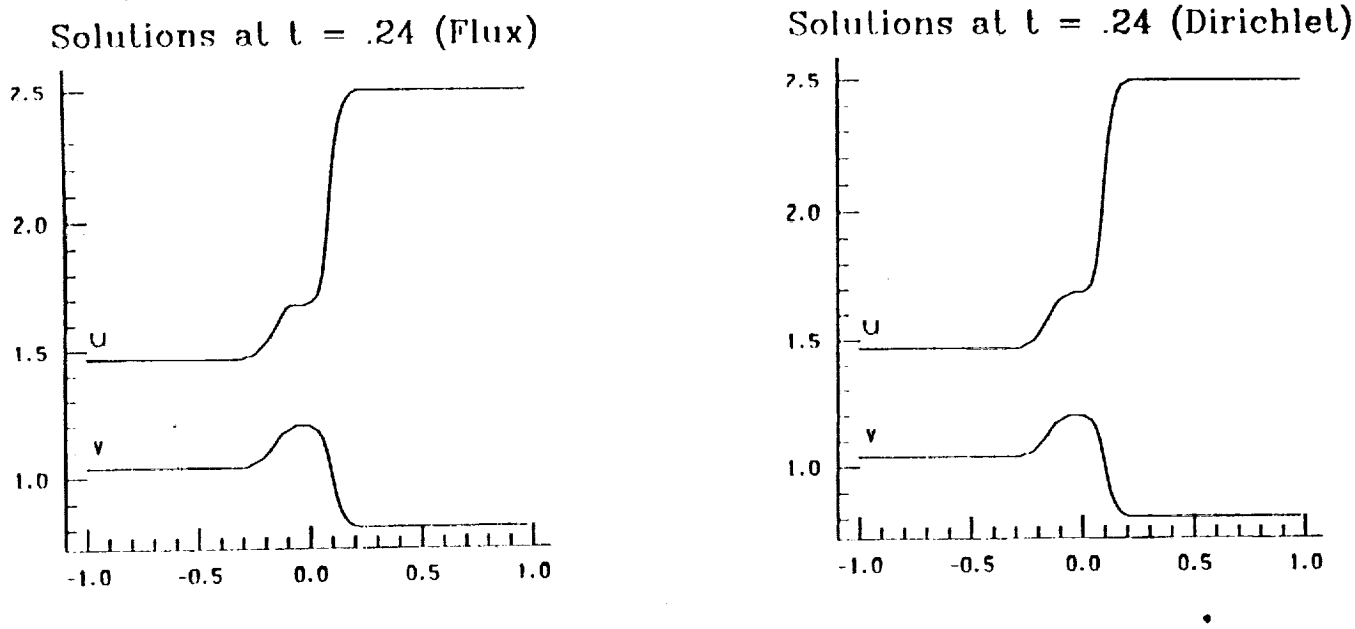

Figure 6.3: Solution on Coarse Mesh at $t = .24$.

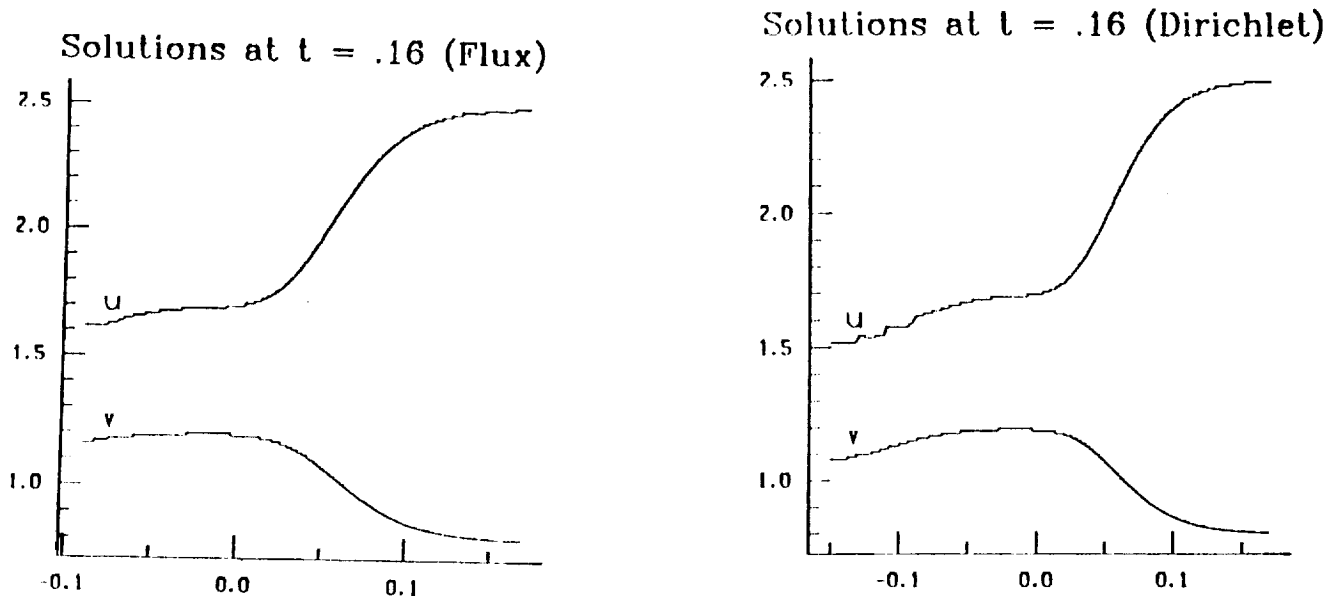

Figure 6.4: Solution on Fine Mesh at $t = .16$.

References

[1] A. Bourgeat and M. Garbey, *Computation of viscous (or nonviscous) conservation law by domain decomposition based on asymptotic analysis*, Preprint 86, equipe d' analysie numerique, LYON-St Etienne, September 1989.

[2] A. Quateroni, G. S. Landriani, and A. Valli, *Coupling of viscous and inviscid stokes equations via a domain decomposition method for finite elements*, Tech. Report UTM 287, Dipartimento di Mathematica, Universita delgi Studi di Trento, Provo, Italy, October 1989.

[3] C. Conley and J. Smoller, *Topological methods in the theory of shock waves*, in Proc. Symposium on Pure Mathematics, Providence, 1973, pp. 233–302.

[4] F. Gastaldi, A. Quateroni, and G. Sacchi Landriani, *On the coupling of two dimensional hyperbolic and elliptic equations: analytical and numerical approach*, Tech. Report Quaderno n. 10/89, Dipartimento di Mathematica, Universita' Cattolica del Sacro Cuore, Brescia, Italy, March 1989.

[5] J. S. Scroggs and D. C. Sorensen, *An asymptotic induced numerical method for the convection-diffusion-reaction equation*, in Mathematics for Large Scale Computing, J. Diaz, ed., Marcel Dekker, 1989, pp. 81–114.

[6] M. Garbey, *Singular perturbation problem governed by system of conservation laws*, 1990.

[7] Marc Garbey and Jeffrey S. Scroggs, *Asymptotic-induced method for conservation laws*, in Proceedings for the Workshop on Asymptotic Analysis and Numerical Solution of Partial Differential Equations, H. Kaper and M. Garbey, eds., New York, New York, 1990, Marcel Dekker, pp. 75–98.

[8] Marsha J. Berger and Phil Colella, *Local adaptive mesh refinement for shock hydrodynamics*, Journal of Computational Physics, 82 (1989), pp. 64–84.

[9] Q. V. Dinh, R. Glowinski, J. Periaux, and G. Terrason, *On the coupling of viscous and inviscid models for incompressible fluid flows via domain decomposition*, in First International Symposium on Domain Decomposition Methods for Partial Differential Equations, R. Glowinski, G. H. Golub, G. A. Meurant, and J. Periaux, eds., Philadelphia, 1988, SIAM, pp. 350–369.

[10] R. C. Y. Chin, G. W. Hedstrom, J. R. McGraw, and F. A. Howes, *Parallel computation of multiple-scale problems*, in New Computing Environments: Parallel, Vector, and Systolic, A. Wouk, ed., SIAM, Philadelphia, 1986, pp. 136–153.

[11] Stanley Osher and R. Sanders, *Numerical approximations to nonlinear conservation laws with locally varying time and space grids*, Math. Comp., 41 (1983), pp. 321–336.

One-Way Nesting for a Primitive Equation Ocean Model

D.W. Blake
Naval Oceanographic and Atmospheric Sciences Research Laboratory
Stennis Space Center, MS 39529-5004

Prognostic numerical models for atmospheric and oceanic circulations require initial fields, boundary conditions, and forcing functions in addition to a consistent set of partial differential equations, including a state relation and equations expressing conservation of mass, momentum and energy. Depending on the horizontal domain to be modeled, the horizontal boundary conditions are either physically obvious or extremely difficult to specify consistently. If the entire atmosphere is modeled, periodic horizontal boundary conditions are appropriate. On the other hand, the physical horizontal boundaries on the entire ocean are solid walls. Obviously, the normal velocity at a solid wall is zero while the specification of the tangential velocity depends on the mathematical treatment of the horizontal viscous terms. Limitations imposed by computer capacity and cost, as well as research interests, have led to the use of limited area models to study flows in the atmosphere and ocean. The limited area models do not have physical horizontal boundaries, merely numerical ones. Correctly determining these open boundary conditions for limited-area numerical models has both intrigued and frustrated numerical modelers for decades.

One common approach is to use the closed or solid wall boundary conditions for a limited-area model. The argument given for this approach is that the boundary conditions affect flow near the walls but that none of these effects are propagated into the interior. Therefore, one chooses a big enough domain that the central region of interest is not corrupted by the boundary flow. Research in progress to model the North Atlantic circulation (J. D. Thompson, private communication) vividly illustrates the pitfalls of this approach. The area covered by the Atlantic Ocean model lies between longitudes 0 and 100W and between latitudes 60N and 20S with the continental boundaries in place as appropriate and the open water boundaries artificially closed. Two model runs are compared: (A) The southern boundary at 20S between latitudes 0 and 40W is artificially closed and (B) the same boundary is specified as open with an inward transport of 15 *Sv* (determined from a global model with the same physics) uniformly spread across the boundary. Comparison of runs A and B shows significant differences. For example, the maximum eddy kinetic energy (divided by the mean density) is 700 cm^2/sec^2 in run A while that for run B is 1900 cm^2/sec^2. The Gulf Stream in run B detaches from the eastern boundary of the United States at the correct latitude of approximately 40N while the Gulf Stream in run A never truly flows along the eastern boundary of the United States at all. The circulation in the tropics and along the eastern boundary of South America also differs radically between the two runs. There are regions in the two runs where there is no difference but such regions are small and of little interest, i.e. they have very low eddy kinetic energy. These studies and others indicate that the interior flow of limited-area models can be dramatically affected by the incorrect use of closed boundary conditions.

A second common approach is to "nest" the limited-area model inside of another numerical model which covers a much larger domain. The outer domain model then supplies the boundary conditions at the open boundaries of the inner domain or limited-area model. As an example, the North Atlantic model described above could have boundary information supplied by a global ocean model which has physical, solid walls or closed boundaries. The outer domain model usually has a larger time step and coarser mesh size than the inner domain model. If the inner and outer domain models are described by the same differential equations and assumptions, then the nesting problem is homogeneous. Otherwise, the nesting problem is heterogeneous. The nesting is described as two-way if information passes from the outer domain to the inner domain and vice-versa. If the outer domain model passes information to the inner domain but the inner domain information is not passed into the outer domain, then the nesting is one-way. Only one-way nesting with a homogeneous system of numerical models is presented here although future work with two-way (or coupled) nesting and with heterogeneous model systems is planned.

In general, nesting involves two separate problems. The first is the interpolation of information from a coarse mesh, outer domain, to a finer mesh, inner domain. The second is the modification of the information supplied by the outer domain before it is applied to the boundary of the inner domain. Much of the research done to date has not distinguished between these two separate problems.

Linear interpolation is the easiest interpolation method to use. However, linear interpolation alters the long wavelength information contained in the original fields and adds short wavelengths that are not present at all in the original fields. Thus, linear interpolation alters the energy distribution of the original fields. To avoid these problems, a variation of the resampling method commonly used by engineers in the time-frequency domain (B.E. Eckstein, private communication) has been tested. A fast Fourier transform (D.N. Fox, private communication) has been modified so that the output fields, after the inverse Fast Fourier Transform, have the required fine grid mesh, although the input fields were supplied on the coarse grid mesh. After testing, this technique was modified (A. Wallcraft, private communication) to handle irregular coastal geometry, which also has to be interpolated. This interpolation scheme has been used extensively with the Pacific Basin numerical models to avoid the lengthy and expensive new spin-ups required whenever the mesh size is changed. (Further discussion of the Pacific Basin research can be found in Hurlburt et al. [1]).

The effects of changing the mesh size are similar in many ways to those found by changing the coefficient of horizontal eddy viscosity, A_H. Therefore, in order to avoid interpolation effects, the open boundary conditions are studies using models with different coefficients of horizontal viscosity. There are three model runs to be considered here. The *applied* run is made with the large outer domain and with a large value of A_H. The *nested* run is made with the small inner domain and a small value of A_H. The *true* run is made with the large outer domain and with a small value of A_H. The boundary conditions applied on the open boundaries of the small domain are taken from the matching grid points on the outer domain and "adjusted" as described below.

The numerical ocean model used for both the inner and outer domain is a reduced gravity, one active layer, primitive equation model with the hydrostatic approximation used. The fluid is assumed to be incompressible with uniform density in each layer. The effects of the density difference between the two layers is ignored except when multiplied by the earth's gravitational acceleration. The prognostic equations for the horizontal components of momentum are written in transport form while the continuity equation is the prognostic equation for the layer-depth of the upper, active layer. A spherical coordinate system is used and the effects of the earth's rotation are included. For further details of these equations in analytic form, see Hurlburt and Thompson [2]. This ocean model will be referred to as the NOARL model.

The outer domain used is a rectangle. The wind forcing is analytic and drives a double gyre in the ocean model. This choice permits the placement of the inner domain to isolate various types of flow: normal or tangential to the open boundary, strong or weak, or flow which changes along the open boundary either spatially or temporally (for time-varying forcing). The work presented here has only one open boundary, either on the western or northern boundary of the inner domain, and the other three boundaries are closed, matching the outer domain.

The NOARL ocean model uses a staggered grid to increase the computational accuracy. If solid walls (closed boundaries) are used, then the eastward velocity, u, and the northward velocity, v are set to zero along the solid walls. It follows that the eastward transport, U, and the northward transport, V, must be zero also on the solid walls. For solid walls, no boundary condition for the layer depth, h, is required. needed. If a boundary is open, then initial conditions for all five variables u, v, U, V, and h must be specified to obtain a numerical solution. However, arbitrary specification of these five variables on the open boundary will in general overspecify the solution. In general and in this research, if the inner domain open boundary values are supplied directly from the outer domain with no modification or adjustments, the inner domain model will eventually "blow up", much less give the correct solution.

If the open boundary condition cannot be specified exactly, then the goal is to prevent reflections at the open boundary which quickly destroy the interior solutions. Most nesting work uses some combination of four basic techniques (Koch and McQueen [3]): blending, filtering, damping, and radiation. Damping refers to an increase in the coefficient of eddy viscosity near the open boundary. Filtering, which is used in many numerical models without open boundaries, is the replacement of a calculated value at a given gridpoint with a weighted combination of the calculated value and the surrounding values. Blending is the replacement of the calculated prognostic term near the boundary of the inner grid with a combination of the prognostic term from the inner grid and that from the outer grid. The radiation technique (Sommerfeld [5] and Orlanski [4]) calculates the boundary values, assuming a wave is passing through the boundary. The first three techniques tend to destroy the small scale structure of the inner grid parameters which defeats the main purpose of running the inner grid with increased horizontal resolution. The radiation technique tends to let the waves pass out but

is limited by the problem of calculating the phase speed needed. The question arises as to how the phase speed should be calculated if there are several types of waves present.

The goal of this research is to produce a nesting technique which does not destroy the inner grid solution or reduce any improvements made in the solution by using the finer grid. Therefore, no blending nor any additional damping or filtering has been used on the inner domain. The radiation technique has been modified from that used by Sommerfeld [5] and Orlanski [4]. The wave equation is used, not with an inner grid variable, but with a new variable that is the difference between the inner domain and the outer domain variable, i.e., $Q(inner) - Q(outer)$. The actual open boundary condition used on the open boundary is the sum of the outer domain solution and the q found from the wave equation:

$$\partial q/\partial t + c\partial q/\partial n = 0,$$

where c is the phase speed and n is the direction normal to the boundary. The phase speed used is determined from the mean outflow and the inflow phase speed is set to zero. The mass exchange along the boundary is the same for the inner and outer domains.

The quality of the nesting technique is measured by how well the inner domain solution (the *nested* run) compares with the *true* run (with the outer domain) solution. This difference is compared to the difference between the *true* outer domain solution and the *applied* outer domain solution. The first tests were done with steady forcing and nearly normal outflow. For these cases the differences between the *true* and *nested* solution after a year are less than five percent of the differences between the *true* and the *applied* solutions everywhere except for a very small area near part of the open boundary where the values go up to 20%. This small portion of the open boundary is where both the non-normal flow is the largest and the normal flow reverses sign. Note that this region is confined close to the boundary and does not propagate into the interior of the inner domain. Model runs have been extended for five years. Although the differences between *true* and *applied* runs increase with time, the differences between the *true* and *nested* runs increase much more slowly. Therefore, the percentages cited above actually decrease with longer model runs.

Ongoing research includes testing open boundaries with non-normal flow, strong jets, and reversal of flow with time. Also, the nesting technique is being tested with actual ocean models with irregular coastlines included. Specifically, a tropical Pacific Ocean model has been nested into a Northern Pacific Basin Model for testing.

The results to date include:

- Open boundary conditions that can handle both inflow and outflow grid points.
- Phase speed selection is not crucial for regime tested.
- Horizontal interpolation is more critical than temporal interpolation.

- Five-year nested model runs have been completed.
- Strong tangential flows require both modified h and non-normal treatment of phase speed.
- Differences in variable values between *true* and *nested* runs are, in general, less than 5% of those between *true* and *applied* runs.

References

[1] Hurlburt, H., J. Kindle, E.J. Metzger and A. Wallcraft, 1989: Results from a global ocean model in the Western Tropical Pacific. *Proceedings of the Western Pacific International Meeting and Workshop on TOGA COARE*, by J. Picaut, R. Lukas, and T. Delcroix (Editors), 343–354.

[2] Hurlburt, H., and J.D. Thompson, 1982: The dynamics of the Loop Current and shed eddies in a numerical model of the Gulf of Mexico. *Hydrodynamics of semi-enclosed seas*, by J.C.J. Nihoul (Editor), Elsevier, 243–298.

[3] Koch, S.E., and J.T. McQueen, 1987: A survey of nested grid techniques and their potential for use within the MASS weather prediction model. *NASA Technical Memorandum* 87808, 25 pp.

[4] Orlanski, I., 1976: A simple boundary condition for unbounded hyperbolic flows, *J. Comp. Phys.*, **21**, 250–257.

[5] Sommerfeld, A., 1949: *Partial Differential Equations: Lectures on Theoretical Physics*, **6**, Academic Press.

Nested Ocean Models: Work In Progress

A. Louise Perkins

Massachusetts Institute of Technology

Abstract

This paper details the ongoing work of combining three existing software programs into a nested grid oceanography model. The HYPER domain decomposition program [8], the SPEM ocean modeling program [5] and a Quasi-Geostrophy model written in England are being combined into a general ocean modeling facility. This facility will be used to test the viability and the capability of two-way nested grids in the North Atlantic.

1 Introduction

We are beginning work on a basin wide coarse grid overlaid with finer grids that follow major mesoscale and dynamic features in the North Atlantic basin. The grid management will be handled by the HYPER domain decomposition program [8]. We will consider several combinations of solution methods to be used including nesting a primitive equation fine mesh solution method within another primitive equation coarser grid solution, and a primitive equation fine mesh solution within a coarser quasi-geostrophic model solution.

It is well known that to refine the entire coarse mesh in space for ocean circulation modeling would be inefficient; it would require large amounts of memory and waste processor time in quasi-geostrophic regions. In short, refining the entire coarse mesh is overkill. For explicit time-evolution solution methods of primitive equations the advancement must also be severely refined in time to account for the gravity wave stability constraint. This results in an excessive number of time steps. Alternatively, an implicit solution on a fully refined mesh results in a very large matrix problem.

We are attacking two areas of fundamental ocean modeling directly. The efficiency of the boundary conditions between quasi-geostrophic and primitive equation models should be advanced based on the insight acquired from our hierarchical approach to the nesting experiments. The second fundamental area is ocean modeling in general. Nested basin/regional grids are a new concept for ocean applications, and in this respect oceanographic modeling lags behind atmospheric and aerodynamic modeling. But the success of domain decomposition in these more advanced modeling areas provides encouragement that our research efforts are timely, central and well directed towards new, successful applications.

2 The Navier-Stokes Equations on a Rotating Sphere

To examine the Navier-Stokes equations on a rotating sphere in a rotating reference frame R, let I denote an inertial reference frame, and let r be a radius of that sphere. Then

$$(r_t)|_I = (r_t)|_R + \Omega \times r$$

where $r_t = u$ is velocity and the second term on the right-hand side of the equation is the motion a non-rotating observer would see because of the rotation of the sphere. Then

$$(u_I)_t|_I = (u_R)_t|_R + 2\Omega \times u_R + \Omega \times (\Omega \times r) + \Omega_t \times r.$$

On the right-hand side of this equation the second term is the Coriolis acceleration, the third term is the centripetal acceleration, and the fourth term is the acceleration resulting from any changes in the rotation speed.

For geophysical applications here on Earth this last acceleration term is discarded except for *very* long time scales, and centripetal acceleration can be expressed as a potential,

$$\Omega \times (\Omega \times r) = -\nabla \Theta_c,$$

that then can be added to the gravitational force potential to net a new geophysical force potential.

The total or material derivative of a scalar quantity is the same in both reference frames. Hence the form of the conservation of mass and the thermodynamic equations remains the same.

To estimate the frictional forces F, we could assume a Newtonian fluid with a symmetric Navier-Stokes internal pressure tensor. But this molecular dissipative strength would have an unknown relationship to the dissipative strength of a given mesoscale ocean phenomena. In general, a qualitative description of the transfer of energy and momentum between scales of interest, and not these smaller molecular scales, are parameterized based on known qualitative ocean behavior.

3 Governing Equations

Coupling hydrodynamics and thermodynamics, consider an adiabatic, inviscid fluid. It can be described by conservation of momentum, a continuity equation, and an energy equation coupled with an equation of state. That is,

$$\frac{d}{dt}u + \alpha \nabla P + F = 0$$

$$\frac{d}{dt}\alpha - \alpha \nabla \cdot u = 0$$

$$\frac{d}{dt}P + P\gamma \nabla \cdot u = 0$$

where $u \in R^3$ is the velocity, α is the specific volume, P is the pressure, and γ is the ratio of specific heats. Here F is the Coriolis and gravity forces, and $\frac{d}{dt} = \frac{\partial}{\partial t} + u \cdot \nabla$ is the total time derivative.

3.1 Primitive Equations

The hydrostatic approximation neglects vertical acceleration in the vertical equation of motion;

$$\frac{\partial P}{\partial z} = \frac{-g}{\alpha}.$$

The Boussinesq approximation replaces density with a zeroth order mean density everywhere except where multiplied by gravity. The combined hydrostatic and Boussinesq approximations are used to formulate a set of reduced equations known as the primitive equations.

These equations are as follows:

$$\frac{d}{dt}u_H + \alpha\nabla_H P + F_H = 0$$

$$\alpha\frac{\partial P}{\partial z} + g = 0$$

$$\frac{d}{dt}\alpha - \alpha\nabla \cdot u = 0$$

$$\frac{d}{dt}P + P\gamma\nabla \cdot u = 0$$

where $u_H = (u_1, u_2)^t$, $u = (u_H, w)^t$,$\nabla_H = (\frac{\partial}{\partial x_1}, \frac{\partial}{\partial x_2})^t$.

3.2 Geostrophy

Geostrophy, or geopotential flow, retains only the balance between the Coriolis force and the potential field. Geostrophy:

$$fv = g\eta_x$$

$$fu = -g\eta_y$$

is the first approximation in an asymptotic expansion of the primitive equations. Here η is the variation of the sea surface height, a measure of pressure.

3.3 Quasi-Geostrophy

Large-scale ocean movement is typically quasi-geostrophic. Asymptotically, quasi-geostrophic motion has time scales not smaller than the advective time scale. It is geostrophic to lowest order, yet retains dynamics. Velocity fields can change, but they do so in continuous geostrophic balance with pressure. Hence there are temporal derivatives retained. The quasi-geostrophic equations are

$$u_t - fv = -g\eta_x$$

$$v_t + fu = -g\eta_y$$

$$\eta_t + (uH)_x + (vH)_y = 0.$$

Here $H + \eta$ is the mean height, H, plus the variation of thickness η.

4 Related Research

Spall and Holland in unpublished work nested a primitive equation model within a quasi-geostrophic model. They found that the quasi-geostrophic boundary conditions seriously dampened the primitive equation physics close to the boundary, reducing them to essentially quasi-geostrophic physics in the boundary region. Reducing or eliminating this boundary layer is the principle focus of our current efforts.

Thompson and Schmitz [7] varied the damping time scale on outflow boundary conditions for a model of the gulf stream. They found that the outflow dynamics and hence the location of the Gulf stream are significantly impacted by the outflow boundary conditions. With such strong impact, the possibility of numerical artifacts in regional models due to boundary conditions seems large. The lack of existence of well-posed boundary conditions for primative equations complicates this problem because no comparisons with true boundary conditions can be made even as approximations [7]. See the article by Dr. Blake in this proceedings for more detailed information.

This leads to the importance of getting the boundary conditions *physically* correct. It is known that the subcharacteristics of the Euler equations, upon which the primitive equations are based, can have combined inflow and outflow characteristics at both advective inflow and outflow boundaries, dependent on the sound speed. Hence the dynamics of the refined regions typically has an affect on the surrounding flow fields. Using one-way boundary conditions for inflow and one-way for outflow is not, in general, sufficient. There must be a stronger interaction between the dynamics of the coarse and the refined meshes.

To strengthen the interaction Spall and Holland [9] added a direct, but averaged, insertion of the streamfunction field (generated using the refined primitive equation depth-averaged horizontal velocity values on the refined mesh) onto the coarser quasi-geostrophic solution. They allow the refined mesh to dictate the regional external flow component.

Our hypothesis is that the external flow is insufficient. The strong dynamics in the gulf stream are forced by internal instabilities. We are currently testing both baroclinic and barotropic nudging for all prognostic variables to establish a stronger relationship between the regional dynamics and the coarse mesh solution behavior. This will be done while maintaining Spall and Hollands quasi-geostrophic to primitive equation boundary conditions [9], which are barotropic, to see if we can improve upon their results. If we are successful, we will experiment with a quasi-geostrophic coarse mesh solution and try to find more comprehensive two-way communication techniques that reduce or eliminate the boundary layer formation found in the previous work.

We are currently using the barotropic modon defined in [9], and a baroclinic vortex problem.

We are working with flat topography at first, so that we can combine either fixed or sigma (stretched) vertical coordinate models.

5 Initial Boundary Value Problems

For modeling purposes these equations must, of course, be viewed as initial boundary-value problems (IBVP). Computational models use IBVP for hindcasts, nowcasts, and forecasts as well as for physical studies that examine phenomena of interest such as energy cascades, eddy shedding, and coastal upwelling. There are two prevalent boundary conditions used in ocean models: rigid walls and open boundary conditions. The trick, of course, is to find open boundary conditions that are well posed and yet not overconstrained. Because one cannot simultaneously diagonalize the coefficient matrices for the multidimensional advective terms of the Navier-Stokes equations, this is often a time-consuming guessing game.

To define open boundary conditions in general, define a system of equations

$$Lu = F$$

with given initial conditions

$$u(x : t = 0) = u_0(x)$$

and characteristic boundary conditions

$$u^1 = Su^2 + g$$

where $u = (u^1, u^2)^t$ are the prognostic variables, and S is a generalized reflection operator [4].

But for reduced equations there can also be modeling constraints such as hydrostatic balance or incompressibility. The modeling constraints assumed in order to reduce the equations (that is, the asymptotic balances chosen) must be enforced on the initial conditions and the boundary conditions to avoid introducing inappropriate length and time scales.

Many obvious well-posed boundary conditions are overspecified, which leads to the formation of boundary layers within which the solution adjusts to the additional information.

5.1 Open Boundary Conditions

The major issue to address is boundary conditions. Oliger and Sundstrom in [4] detail some boundary treatment for geophysical problems, and show that point-wise local boundary conditions for the primitive equations are not well-posed: the regional open boundary problem is open-ended. It is not known, however, whether non-local boundary conditions, such as those generated with a domain decomposition method where boundary conditions that are derived from a larger domain are or are not well-posed. We may have fewer problems with open boundary conditions at a two-sided boundary. The quasi-geostrophic boundary layer within the nested primitive equation model in the unpublished work of Spall and Holland indicate that open boundary conditions on a nested grid is a major problem that must be addressed before two-way nesting will be successful.

Our approach has been to work from the primitive equation homogeneous model backwards to the quasi-geostrophic model, assessing the differences in the information transmitted across boundaries, to derive better open boundary conditions for the simplier quasi-geostrophic model.

For the heterogeneous boundary conditions between the primitive equation and quasi-geostrophic regions the quasi-geostrophic boundaries need to evolve as if there was primitive equation physics in the region surrounding the refined domain. To insure this we are monitoring $\frac{\partial \rho}{\partial t}$ on the boundary, where quasi-geostrophic physics, which is less vertically diverse, is statically stable, and comparing the evolving quasi-geostrophic boundary against a fine mesh primitive equation global solution. This is one of our measures of error that is physically based.

6 HYPER

The HYPER program, described in Perkins [5], looks at domain decomposition as a tool to combine grids for computational efficiency and for model flexibility. It currently can locate where refined grids should be placed based on asymptotic and-or physical criteria and it initializes the refined grids using local uniform mesh refinement.

Our current work is a static domain decomposition; we are running experiments on the influence of the internal boundaries on the flow pattern, and are interested in the flow through that boundary. These results are currently being prepared and will appear in a later report.

The goal is to follow different asymptotic regimes within the ocean basin that are identifiable as distinct physical regions of the ocean. The problem is that, once you're inside a reduced physics region, such as a quasi-geostrophic region where there is no ageostrophic flow, there may be no way for the model to evolve the complete physics you hope to recover by using the refined meshes. For example, in the gulf stream region meanders pinch off to form eddies. Many aspects of the physics contribute to this pinching off. In such cases the reduced quasi-geostrophic model will not reproduce the ageostrophic behavior in the initial conditions of the refined mesh, and hence will miss some of the time dependent interactions that contribute to the dynamically significant event of ring shedding. There will be no ageostrophic signals in the initial conditions to interpolate onto the refined mesh. In such a situation, the data used to help initialize the model may make up for some of the missing physics, but the time scales may be off.

7 Domain Decomposition

Domain decomposition allows the mesh to evolve with the solution. It has been applied to elliptic and hyperbolic equations for several years. The interested reader can refer to Chan, et al., [2] for an extensive bibliography on elliptic and hyperbolic domain decomposition methods.

Formally we describe the domain decomposition of a discrete coarse mesh, Ω^1, on the computational mesh Ω, for a fixed time $t = n\Delta t$, by letting $(p(t) - 1)$ be the number of

refined subdomains used at time t and $\{\Omega^k\}_{k=2}^{p(t)}$ be those subdomains:

$$\bigcup_{k=1}^{p(t)} \Omega^k(t) \subset \Omega .$$

After the domain is decomposed, local uniform spatial mesh refinement, as developed by Berger [1], is applied to the new subdomains. The time step may also be refined on these regions.

The sequencing for one coarse time step of magnitude $\Delta_c t$ from time t^n to time $t^n + \Delta_c t$, where n indexes the discrete time steps on the coarse mesh, is presented next. Let the temporal refinement ratio from the coarse mesh to the refined meshes be r, and notate this $r\Delta_f t = \Delta_c t$, so that a subscript "c" informs us that we are on the coarse mesh, and a subscript "f" informs us that we are discussing one of the refined meshes. The domain decomposition algorithm follows:

Domain Decomposition Algorithm

```
Advance coarse mesh
Mark points with significant mesoscale and ageostrophic potential
Cluster these points into refined meshes
DO r times
    Solve equations on refined meshes
ENDDO
Nudge refined values onto coarse mesh
```

When all of the refined meshes have been advanced r refined time steps to the next coarse time step, their values at time t^{n+1} are passed to the coarse mesh where a nudging technique modifies the coarse advanced values and produces an aggregate solution on the coarse mesh. Let F^A, F^1, and $\{F^k\}_{k=2}^{p(t)}$ represent the discrete operators for the aggregate solution on the original discretized mesh Ω^1, the solution on the coarse mesh Ω^1, and the separate solutions on each of the refined subdomains $\{\Omega^k\}_{k=2}^{p(t)}$, respectively. Then the aggregate solution on the coarse discretized mesh is given by

$$F^A(\Omega^1) = C\left[\{F^k(\Omega^k)\}_{k=2}^{p(t)}, F^1(\Omega^1)\right] \qquad (7.1)$$

where the operator C is a nudging technique that may vary between experiments.

We use domain decomposition as a tool to combine the explicit coarse mesh solution method with the refined mesh solution methods to satisfy our varying numerical requirements in a computationally efficient way. We use a two-level refinement scheme consisting of one coarse mesh and a set of overlaid refined meshes, where the coarse mesh adequately represents quasi-geostrophic behavior, while the refined meshes adequately resolves the more physically complete primitive equations.

Refined to coarse mesh communication (feedback) can take the form of value averaging, as in Berger [1] and as in Spall and Holland [6].

We are using a nudging data assimilation technique for the initial experiment and we do not include explicit conservation enforcement.

Our domain decomposition work focuses on two-way interactive nested grid communications and the development of good internal boundary conditions. We are particularly interested in examining heterogeneous open boundary conditions between different asymptotic regions. Because the major geophysical equations are not known to be well-posed as an initial value boundary problem, in general, this issue becomes important.

8 Initial Conditions

Our long range plans are to build a basin wide grid, and overlay it with refined grids about regions of ageostrophic dynamic regions. The refined grids will then follow mesoscale or planetary scale dynamical features.

But our current work is much less ambitious. We have constructed a box model and are using Spall and Hollands [12] barotropic modon and baroclinic vortex problems to examine the viability and desirability of different communication schemes between the coarse and refined meshes.

A barotropic modon is a coherent, concentric streamfunction. The barotropic flow is the primary mode of a quasi-geostrophic equation formulated as a Sturm-Liouville problem (all other modes of the Sturm-Liouville problem are referred to as baroclinic). It has an analytic solution, it is quasi-geostrophic, and uses an infinite beta plane approximation. The result is a coherent depth independent (barotropic) structure that moves at constant speed.

The baroclinic vortex has no analytic solution, and is defined using a Gaussian pressure distribution with maximum geostrophic velocity of $100 cm/sec$. The initial velocity fields are calculated to be in geostrophic balance with the prescribed Gaussian pressure field.

Our experiment follows a hierarchical approach. Beginning with a homogeneous domain decomposition we use a full, coarse primitive equation model and keep track of the flow across the "future" internal boundaries. Then we introduce the nested grid into the same problem and analyze any changes in the boundary information flow. This is used as our error due to boundary conditions only. This error is measured both in root mean squared error and in phase error. Small shifts of mesoscale features are not always bad compared to changes in dynamics within those mesoscale features.

Once we complete our homogeneous studies we will move to a heterogeneous domain decomposition with a quasi-geostrophic coarse grid overlaid with a primitive equation refined grid. Again we will compare the flow across the internal boundaries. Then we will add a feedback loop that uses the nudging data assimilation technique from the refined mesh to the coarse mesh and nudge to the true boundary information. This way we can measure the improvement due to the nudging feedback loop.

The quasi-geostrophic coarser model will be forced by the nudging from the refined primitive equation model. The unforced quasi-geostrophic model is statically stability, but the

primitive equation is not. The forced behavior perturbs the reduced equation dynamics, so that a time series of its behavior in the refined region will not be statically stability due to the feedback interaction. But with known density changes at the boundaries from our true solution, we can measure how well the reduced dynamics are being influenced by the regional models with their more complete physical models. Another metric is the apparent ageostrophic time series behavior in the quasi-geostrophic coarser model. After nudging, the ageostrophic adjustment to the quasi-geostrophic coarse mesh is calculated, and a time series of this difference is the ageostrophic forcing of the quasi-geostrophic model. Where this difference is small, there is no need to maintain a refined mesh, so this metric can be used to eliminate refined meshes that are no longer needed, but it can not help us locate where refined meshes should be placed.

8.1 Semi-Spectral Primitive Equation Model (SPEM)

The primitive equation SPEM model of Haidvogel et. al. [3] has prognostic variables for horizontal velocity, u and v, and temperature t, and salinity s. It uses the hydrostatic and Boussinesq approximation. The resulting equations are advanced on an scattered Arakawa "C" grid in the horizontal, while the vertical is spectral, with Chebyshev modes. It has a rigid lid approximation at the surface (no variations or "waves" in sea surface height).

9 Current Summary

The computational demands of fully three-dimensional global ocean modeling seem to require a nested heterogeneous adaptive grid solution. However, the implementation difficulties are robust. The need for physically realistic open boundary conditions is already well documented, mostly a result of a "grand challenge" issued several years ago. Our experience indicates that an equally pressing need is to provide modeling-consistent asymptotically nested initial conditions for each new nested grid.

The scientific aspects of the work are focused on the boundary condition formulation and on the two-way grid communication mechanisms under development.

References

[1] M.J. Berger, *Adaptive Mesh Refinement For Hyperbolic Partial Differential Equations*, Ph.D. Dissertation, Stanford University, 1982.

[2] Chan, T.F., R. Glowinski, J. Periaux, and O.B. Widlund, eds, *Domain Decomposition Methods*, SIAM, 1989.

[3] Haidvogel, Wilkin, and Young, *A semi-spectral primitive equation ocean circulation model using vertical sigma and orthogonal curvi-linear horizontal coordinates*, JCP, 1989, in press.

[4] J. Oliger and A. Sundstrom, *Theoretical and practical aspects of some initial boundary value problems in fluid dynamics*, SIAM J. Appl. Math. **35**, no. 3 (1978) 419–446.

[5] Perkins, A.L.,*Parallel Heterogeneous Mesh Refinement For Multidimensional Convection-Diffusion Equations Using An Euler-Lagrange Method*, Ph.D. Dissertation, UCRL-53950, 1989.

[6] Spall, M.A., and W.R. Holland, *A Nested Primitive Equation Model For Oceanic Applications*, to appear in J. Phys. Ocean.

[7] Thompson, J.D., and W.J. Schmitz, *A Limited-Area Model of the Gulf Stream: Design, Initial Experiments, and Model-Data Intercomparison*, J. Phys. Ocean., Vol. 19, No. 6, June 1989.

OMIT 70
END

Heterogeneous Domain Decomposition Bibliography

Compiled By

Jeffrey S. Scroggs
Department of Mathematics
North Carolina State University
Raleigh, North Carolina
and
A. Louise Perkins
Department of Earth, Atmospheric and Planetary Sciences
Massachusetts Institute of Technology
Cambridge, Massachusetts

1 Introduction

The activity in research of domain decomposition for the numerical solution of partial differential equations is increasing at a rapid pace. One motivation for domain decomposition is the isolation of physical phenomenae into separate subdomains. The numerical treatment (and possibly even the modeling equations) may be different in these subdomains. Thus, this style of domain decomposition is *heterogeneous*.

This bibliography includes references to works central to the development of heterogeneous domain decomposition.

The bibliography is by no means complete. Indeed, we would be delighted to receive additional references to add to the bibliography.

2 Adding to this Bibliography

We would like additional references that are core to the topic of heterogeneous domain decomposition. Please use the following guidelines:

Format	Bibliographic data should be in bibtex format. A set of keywords is requested as part of the format. These keywords will be used to form the index portion of this database.
Medium	Email messages to Louise Perkins or Jeff Scroggs.
Assistance	To assist with placing the data in bibtex format, send a request to either of us for the C program BIBINPUT. This program will interactively prompt you for the data, and produce a file with the formatted entries.

Disclaimer We are trying to keep this bibliography focused, hence submissions that do not obviously deal with heterogeneous domain decomposition will be eliminated.

Please send your references to

Louise Perkins
54-1420
MIT
Cambridge, MA 02139
(617)253-1291
perkins@pimms.mit.edu

or

Jeffrey S. Scroggs
Box 8205
Department of Mathematics
North Carolina State University
(919)737-7817
scroggs@matjfs.ncsu.edu

3 Index

References

[1] Ø. ANDREASSEN AND I. LIE, *Numerical simulation of propagation and interaction of acoustic and elastic waves in two different media*, Tech. report 91/7020, NDRE, Div. for Electronics, P.O.Box 25, N-2007 Kjeller, Norway, March 1991.

[2] H. S. BERRYMAN, J. SALTZ, AND J. S. SCROGGS, *Execution time support for adaptive scientific algorithms on distributed memory machines*, ICASE Report 90-41, ICASE, NASA Langley Research Center, Hampton, Virginia 23665-5225, 1990.

[3] A. BOURGEAT AND M. GARBEY, *Computation of viscous (or nonviscous) conservation law by domain decomposition based on asymptotic analysis*, Preprint 86, equipe d' analysie numerique, LYON-St Etienne, September 1989.

[4] D. L. BROWN, L. G. M. REYNA, AND L. GUILLERMO, *A two-dimensional mesh refinement method for problems with one-dimensional singularities*, SIAM J. Sci. Stat. Comp., 6 (1985), pp. 515–531.

[5] R. C. Y. CHIN, G. W. HEDSTROM, AND F. A. HOWES, *Considerations on solving problems with multiple scales*, in Multiple Time Scales, J. U. Brackbill and B. I. Cohen, eds., Academic Press, Orlando, Florida, 1985, pp. 1–27.

[6] R. C. Y. CHIN, G. W. HEDSTROM, J. R. MCGRAW, AND F. A. HOWES, *Parallel computation of multiple-scale problems*, in New Computing Environments: Parallel, Vector, and Systolic, A. Wouk, ed., SIAM, Philadelphia, 1986, pp. 136–153.

[7] R. C. Y. CHIN, G. W. HEDSTROM, J. S. SCROGGS, AND D. C. SORENSEN, *Parallel computation of a domain decomposition method*, in IMACS 6th International Symposium on Computer Methods for Partial Differential Equations, 1987.

[8] GEORGES-HENRI COTTET, *A particle-grid superposition method for the Navier-Stokes equations*, 1989.

[9] Q. V. DINH, R. GLOWINSKI, J. PERIAUX, AND G. TERRASON, *On the coupling of viscous and inviscid models for incompressible fluid flows via domain decomposition*, in First International Symposium on Domain Decomposition Methods for Partial Differential Equations, R. Glowinski, G. H. Golub, G. A. Meurant, and J. Periaux, eds., Philadelphia, 1988, SIAM, pp. 350–369.

[10] A. FRATI, R. PASQUARELLI, AND A. QUATERONI, *Spectral approximation to advection-diffusion problems by the fictitous interface method*, Tech. Report UMSI 90/213, University of Minnesota, Minneapolis, Minnesota, October, 1990.

[11] M. GARBEY, *Quasilinear hyperbolic-hyperbolic singular perturbation problem: Study of a shock layer*, Mathematical Methods in the Applied Sciences, 11 (1989), pp. 237–252.

[12] M. GARBEY, *Asymptotic analysis of singular perturbation problems governed by a conservation law*, Preprint MCS-P107-1089, MCS, Argonne National Lab, October 1989.

[13] M. GARBEY AND D. LEVINE, *Massively parallel computation of conservation laws*, Preprint MCS-P85-0689, MCS, Argonne National Lab, June 1989.

[14] MARC GARBEY AND JEFFREY S. SCROGGS, *Asymptotic-induced method for conservation laws*, in Proceedings for the Workshop on Asymptotic Analysis and Numerical Solution of Partial Differential Equations, H. Kaper and M. Garbey, eds., New York, New York, 1990, Marcel Dekker, Inc., pp. 75–98.

[15] F. GASTALDI, A. QUATERONI, AND G. S. LANDRIANI, *Effective methods for the treatment of interfaces separating equations of different character*, in CMEM meeting, Capri, May 23-26, 1989.

[16] F. GASTALDI, A. QUATERONI, AND G. SACCHI LANDRIANI, *On the coupling of two dimensional hyperbolic and elliptic equations: Analytical and numerical approach*, Tech. Report Quaderno n. 10/89, Dipartimento di Mathematica, Universita' Cattolica del Sacro Cuore, Brescia, Italy, March 1989.

[17] G. W. HEDSTROM AND F. A. HOWES, *A domain decomposition method for a convection diffusion equation with turning points*, in Domain Decomposition Methods, T. F. Chan, R. Glowinski, J. Periaux, and O. B. Widlund, eds., Philadelphia, 1989, SIAM, pp. 38–46.

[18] G. SACCHI LANDRIANI AND A. QUATERONI, *Iteration by subdomains in numerical fluid dynamics*, Tech. Report Quaderno n. 9/89, Dipartimento di Mathematica, Universita' Cattolica del Sacro Cuore, Brescia, Italy, March 1989.

[19] I. LIE, *Ocean/bottom acoustic interaction with arbitrary bottom profile*, Tech. report 91/7022, NDRE, Div. for Electronics, P.O.Box 25, N-2007 Kjeller, Norway, March 1991.

[20] A. L. PERKINS, *Parallel Heterogeneous Mesh Refinement For Multidimensional Convection-Diffusion Equations Using An Euler-Lagrange Method*, PhD thesis, University of California, Davis, 1989.

[21] A. LOUISE PERKINS AND GARRY RODRIGUE, *A domain decomposition method for solving a two-dimensional viscous Burgers' equation*, App. Numer. Math., 6 (1990), pp. 329–340.

[22] A. QUATERONI, G. S. LANDRIANI, AND A. VALLI, *Coupling of viscous and inviscid Stokes equations via a domain decomposition method for finite elements*, Tech. Report UTM 287, Dipartimento di Mathematica, Universita delgi Studi di Trento, Provo, Italy, October 1989.

[23] A. QUATERONI AND A. VALLI, *Domain decomposition for a generalized Stokes problem*, Tech. Report UTM 259, Dipartimento di Mathematica, Universita delgi Studi di Trento, Provo, Italy, November 1988.

[24] A. QUATERONI AND A. VALLI, *Theory and application of Steklov-Poincare operators for boundary value problems: the heterogeneous operators case*, Tech. Report UMSI 90/232, University of Minnesota, Minneapolis, Minnesota, November 1990.

[25] A. QUATERONI, *Domain decomposition method for the numerical solution of partial differential equations*, Tech. Report UMSI 90/264, University of Minnesota, Minneapolis, Minnesota, December, 1990.

[26] M. F. RUSSO AND R. L. PESKIN, *Automatically identifying the asymptotic behavior of nonlinear singularly perturbed boundary value problems*, 1989.

[27] J. S. SCROGGS, *A physically motivated domain decomposition for singularly perturbed equations*, SIAM Journal on Numerical Analysis, (to appear, 1990).

[28] J. S. SCROGGS, *The Solution of a Parabolic Partial Differential Equation via Domain Decomposition: The Synthesis of Asymptotic and Numerical Analysis*, PhD thesis, University of Illinois at U-C, 1988.

[29] J. S. SCROGGS., *A parallel algorithm for nonlinear convection-diffusion equations*, in Proceedings for SIAM Conference on Domain Decomposition, SIAM, 1989.

[30] J. S. SCROGGS AND J. SALTZ, *Distributed-memory computing of a physically-motivated domain decomposition method*, in Proceedings for SIAM Conference on Domain Decomposition, SIAM, 1990.

NASA

Report Documentation Page

1. Report No.	2. Government Accession No.	3. Recipient's Catalog No.
NASA CR-187630 ICASE Interim Report 19		

4. Title and Subtitle	5. Report Date
PROCEEDINGS FOR THE ICASE WORKSHOP ON HETEROGENEOUS BOUNDARY CONDITIONS	August 1991
	6. Performing Organization Code

7. Author(s)	8. Performing Organization Report No.
A. Louise Perkins Jeffrey S. Scroggs	Interim Report No. 19
	10. Work Unit No.
	505-90-52-01

9. Performing Organization Name and Address	11. Contract or Grant No.
Institute for Computer Applications in Science and Engineering Mail Stop 132C, NASA Langley Research Center Hampton, VA 23665-5225	NAS1-18605
	13. Type of Report and Period Covered
12. Sponsoring Agency Name and Address National Aeronautics and Space Adminstration Langley Research Center Hampton, VA 23665-5225	Contractor Report
	14. Sponsoring Agency Code

15. Supplementary Notes

Langley Technical Monitor:
Michael F. Card

Final Report

16. Abstract

Domain Decomposition is a complex problem with many interesting aspects. The choice of decomposition can be made based on many different criteria, and the choice of interface of internal boundary conditions are numerous. Even more interesting from a modeling perspective is that the various regions under study may have different dynamical balances, indicating that different physical processes are dominating the flow in those regions. It may be desirable to use different numerical approximations in the regions where the physical processes are dominated by different balances.

The Institute for Computer Applications in Science and Engineering (ICASE), recognizing the need to more clearly define the nature of these complex problems, sponsored this workshop on Heterogeneous Boundary Conditions at the NASA Langley Research Center in Hampton, Virginia. This proceedings is an informal collection of the presentations and discussion groups. It also includes a bibliography that contains many of the references that discuss related topics.

The proceedings begins with summaries of the discussion groups. Then papers describing the talks are presented. Lastly, the bibliography is included, and an index by subject is provided.

17. Key Words (Suggested by Author(s))	18. Distribution Statement
numerical analysis	64 - Numerical Analysis Unclassified - Unlimited

19. Security Classif. (of this report)	20. Security Classif. (of this page)	21. No. of pages	22. Price
Unclassified	Unclassified	80	A05